JOURNAL OF GEOPHYSICAL RESEARCH, VOL. 106, NO. A10, PAGES 21,165–21,181, OCTOBER 1, 2001

# Evolution of electron beam generated waves resulting in transverse ion heating and filamentation of the plasma

N. Singh, S. M. Loo, and B. E. Wells

Department of Electrical and Computer Engineering, University of Alabama in Huntsville, Huntsville, Alabama

G. S. Lakhina

Indian Institute of Geomagnetism, Colaba, Mumbai, India

**Abstract.** We present here a systematic simulational study on electron beam driven waves and their consequences in terms of plasma electrodynamics. The study is performed by using three-dimensional particle-in-cell code, parallelized to simulate a large volume of plasma. Our simulation shows that an initial electron beam of finite radius with beam velocity along the ambient magnetic field triggers a series of events in the evolution of the waves and the plasma. In the initial stage ($t \leq 200\ \omega_{po}^{-1}$, $\omega_{po}$ being the electron plasma frequency with the total electron density $n_0$), high frequency waves near $\omega \sim \omega_{po}$ are driven. These waves progressively disappear giving way to the dominance of lower hybrid (LH) waves. The phase of the lower hybrid waves lasts over the time interval $200 \lesssim t\omega_{po} \lesssim 1000$. In this time period the LH waves stochastically accelerate ions transverse to $\mathbf{B}_o$, and the beam electrons are scattered outside the initial beam volume to occupy the entire volume of the simulation plasma. The ion acceleration leads to the formation of elongated tail in the perpendicular velocity distribution. The large-amplitude LH waves are seen to undergo a parametric decay into resonance cone waves at frequencies $\omega < \Omega_i$, the ion cyclotron frequency. Such extremely low-frequency (ELF) waves are the electrostatic version of the inertial Alfven waves. The phase of the strong LH waves is followed by a stage in which HF waves with frequencies $\omega \sim \omega_{po}$ appear again, but in this stage they are strongly modulated by the already present ELF waves and other low-frequency waves in the frequency range near the ion cyclotron frequency $\Omega_i$ and its harmonics. Beginning with the LH wave stage and continuing into the late stages of ELF waves, the plasma density is highly filamented and the filaments oscillate with the ELF frequencies. The relevance of our results to the observations on plasma waves from satellites is brought out.

## 1. Introduction

The role of lower hybrid (LH) waves in the transverse heating of ions has been known since the mid-1970s in connection with plasma heating in fusion machines [e.g., *Chang and Porkolab*, 1974]. In connection with the observation of the transversely accelerated ions in the auroral plasma [*Klumpar*, 1979], *Chang and Coppi* [1981] suggested that the auroral electron beam driven LH waves might transversely accelerate ions leading to the formation of ion conics. However, *Singh and Schunk* [1984] pointed out that the lower hybrid waves driven by auroral electron beams are too fast to interact with the low-energy ionospheric ions. *Reterrer and Chang* [1988] invoked mode-mode coupling to generate slower waves capable of interacting with cold ions. They also performed one- and two-dimensional (1-D, 2-D) simulations to demonstrate that the LH waves driven by electron beams do indeed heat the ions. However, these simulations with limited dimensionality were specially designed to generate LH waves by fixing the angles of wave propagation suited for such waves while limiting the high-frequency waves, which have much higher growth rates.

Copyright 2001 by the American Geophysical Union.

Paper number 2000JA000335.
0148-0227/01/2000JA000335$09.00

As a matter of fact, there has been a longstanding debate on how an electron beam can drive LH waves when the high-frequency (HF) waves have much higher growth rates (see, e.g., *Singh et al.* [1985]) and quickly plateau the electron beam distribution. It has been suggested that the high-frequency waves with relatively large perpendicular group velocities quickly leave the electron beam of finite perpendicular dimensions, leaving the LH waves to interact with the beam over longer distances because the latter waves have group velocities essentially parallel to the magnetic field (see, e.g., *Chang* [1992]). It has also been suggested that an electron beam in the presence of a hot electron population is not fully plateaued by the high-frequency waves, leaving the possibility of growing LH waves [*Ergun et al.*, 1993; *Muschietti et al.*, 1997]. *Omelchenko et al.* [1994] have suggested the excitation of LH waves by plateaued electron beam distributions via the anomalous electron cyclotron resonance (AECR) [*Mikhailovski*, 1974]. However, the excitation of LH waves by this so-called fan instability requires an excessively large electron beam energy in the auroral plasma.

Singh et al. [1985] performed a parametric study on the excitation of waves by an electron beam by varying the perpendicular wave number $k_\perp$. It was found that only when $k_\perp$ progressively increases above $\rho_i^{-1}$, where $\rho_i$ is the ion Larmor radius, does the growth rate maximize in an

increasingly narrower frequency band just above the LH frequency ($\omega_{lh}$), making the LH wave dominant over the HF waves. However, the question remains regarding the processes which limit the value of $k_\perp > \rho_i^{-1}$. An obvious choice is to limit the transverse size of the electron beam. In this paper we have studied the self-consistent excitation of both low- and high-frequency waves in a plasma driven by an electron beam of finite radius $r_b$ by using a fully 3-D particle-in-cell (PIC) code; we have followed their temporal and spatial evolution. It is shown that during the early stage of the instability the electron beam drives broadband waves in the frequency band $\omega_{lh} \lesssim \omega \lesssim \omega_{po}$ but with dominant peaks in the frequency spectrum (1) just above the LH frequency $\omega_{lh}$, and (2) near the electron plasma frequency $\omega_{po}$. Further evolution leads to the generation of extremely low frequency (ELF) waves at frequencies below the ion cyclotron frequency $\Omega_i = 2\pi f_{ci}$. As the plasma and waves evolve, ions are transversely heated when the LH waves grow to relatively large amplitudes, and the plasma density is highly striated with thin density filaments extending all along the length of the simulation plasma. In the late stage of the evolution, HF waves reappear again but are modulated by a variety of low-frequency waves. The late excitation of HF waves and their modulation are interpreted in terms of the waves driven by the anomalous cyclotron resonance of the electrons in the plateaued beam.

The rest of the paper is planned as follows. In section 2 the simulation model is described. Numerical results are described in section 3. Early time evolution of the plasma waves is discussed in section 3.1, while the late time evolution is addressed in section 3.2. In section 4 we describe the consequence of the waves for the ions and electrons of the plasma showing transverse ion acceleration and transverse spatial diffusion of the beam electrons. Conclusions of the paper along with their relevance to the space plasma are given in section 5.

## 2. Simulation Model

Simulations are performed by using a fully three-dimensional electrostatic parallel PIC code [*Singh et al.*, 1998]. Periodic boundary conditions on both particles and fields were used. We performed several simulations by varying the size of the 3-D simulation volume given by $L_x \times L_y \times L_z$; $L_z$ was fixed at $256\lambda_d$, while $L_x$ and $L_y$ were varied from $16\lambda_d$ to $64\lambda_d$. We chose an electron beam of radius $r_b = 10\lambda_d$ centered at $(L_x/2, L_y/2)$ when $L_x = L_y \geq 32\lambda_d$. In the simulations performed so far, the beam velocity along $z$ parallel to the ambient magnetic field $\mathbf{B}_o$ was assumed to be $V_b = 4V_{te}$ or $8V_{te}$, where $V_{te}$ is the electron thermal velocity. The initial electron and ion temperatures were assumed to be equal, that is, $T_e = T_i = T_o$ and $V_{te} = (k_B T_o / m_e)^{1/2}$, where $k_B$ is the Boltzmann constant and $m_e$ is the electron mass. Beam temperature was varied in different simulations, but as long as $V_b >> V_{te} \gtrsim V_{tb}$, the beam thermal velocity, the actual value of $V_{tb}$ did not matter much. In the runs we used 36 pairs of electrons and ions in each cell of size $\lambda_d^3$. The electron beam density $n_b$ was varied from 5 to 10%. In the simulations described here $n_b = 0.1 n_o$, $n_o$ being the total plasma density. Such a beam density is large for the topside ionosphere, but it is within the observed range in the high-altitude auroral acceleration region (see, e.g., *Cattell et al.* [1998]). The initial plasma carries a current determined by the beam density and velocity, namely, $J = n_b e V_b$. The simulations reported in this paper were performed for ion-to-electron mass ratio $M/m_e = 64$ and $\Omega_e/\omega_{pe} = 2$, where $\Omega_e$ and $\omega_{pe}$ are the electron cyclotron and plasma frequencies, respectively. We have used higher mass ratios such as $M/m_e = 400$ and 1836. For the latter mass ratio and $V_b = 4V_{te}$, the formation of electron holes and their dynamics was reported in an earlier paper [*Singh et al.*, 2000]. The initial wave behavior for all three mass ratios were nearly identical for a given beam. The small mass ratio allowed us to follow the evolution of the plasma and the waves over a long ion timescale, resulting in transverse ion heating and filamentation of the plasma for a relatively large beam velocity $V_b >> V_{te}$, namely, $V_b = 8V_{te}$. On the other hand, for a relatively small $V_b (V_b \cong 4V_{te})$ the late time evolution led to the formation of electron holes [*Singh et al.*, 2000] lasting over a long time as seen in one-dimensional simulations by *Omura et al.* [1996]. In this paper we describe results from the runs with the small mass ratio and large beam velocity, emphasizing (1) generation of both HF and LH waves during the early stage of the beam-plasma interaction, (2) generation of extremely low-frequency waves below the ion cyclotron frequency by the parametric decay of the LH waves, (3) transverse ion heating, (4) diffusion of the beam electrons across the magnetic field, (5) reappearance of HF waves strongly modulated by the ELF and other low-frequency waves, and (6) filamentation of the plasma density when the plasma is driven by a thin electron beam. The reappearance of the HF waves in the late stage is associated with the combined effects of both Cerenkov and anomalous cyclotron resonances of the fast electrons in the plateaued beam.

In our discussions we have used the following normalizations and definitions: distance $\bar{x} = x/\lambda_d$, time $\bar{t} = t\omega_{po}$, velocity $\bar{V} = V/V_{te}$, potential $\bar{\Phi} = \Phi/\phi_n$, and electric field $\bar{E} = \bar{E}/E_n$, where $\lambda_d = V_{te}/\omega_{pe}$, $\phi_n = k_B T_o / e$, $E_n = \phi_n/\lambda_d$ and $\omega_{po}$ is the electron plasma frequency with the total plasma density $n_o$.

## 3. Numerical Results

Figure 1 shows a typical temporal evolution of waves obtained in a simulation which ran up to $\bar{t} = 3000$. In this figure the potential at point $P_1$ (16, 24, 5) is plotted as a function of time. The time series plot contains a variety of waves and their nonlinear interactions. For $\bar{t} \leq 300$, the waves are dominated by high-frequency oscillations, but they are already modulated by some low-frequency oscillations. For $\bar{t} > 300$, the low-frequency oscillations begin to dominate and the HF oscillations appear as an additive noise. But again for $\bar{t} > 900$ the HF oscillations reemerge and they are amplitude modulated by a variety of low-frequency oscillations. Figure 1b shows the frequency spectrum of the oscillations in Figure 1a. Before we discuss the spectrum, we note that in the simulation the ion cyclotron frequency is $\Omega_i \cong 0.03\omega_{po}$, and the lower hybrid (LH) frequency is $\omega_{lh} \cong \omega_{pi}/(1 + \omega_{po}^2/\Omega_e^2)^{1/2} = 0.11\,\omega_{po}$, where $\omega_{po}$ is the electron plasma frequency, $\omega_{pi}$ is the ion plasma frequency, and the electron cyclotron frequency $\Omega_e = 2\omega_{po}$. Figure 1b shows that there are several discrete peaks in the frequency band $\omega_{lh} \leq \omega \leq \omega_{po}$ and an extremely low-frequency broadband component peaking at a frequency $\omega < \Omega_i$. The spectrum shown in Figure 1b is found to represent the power

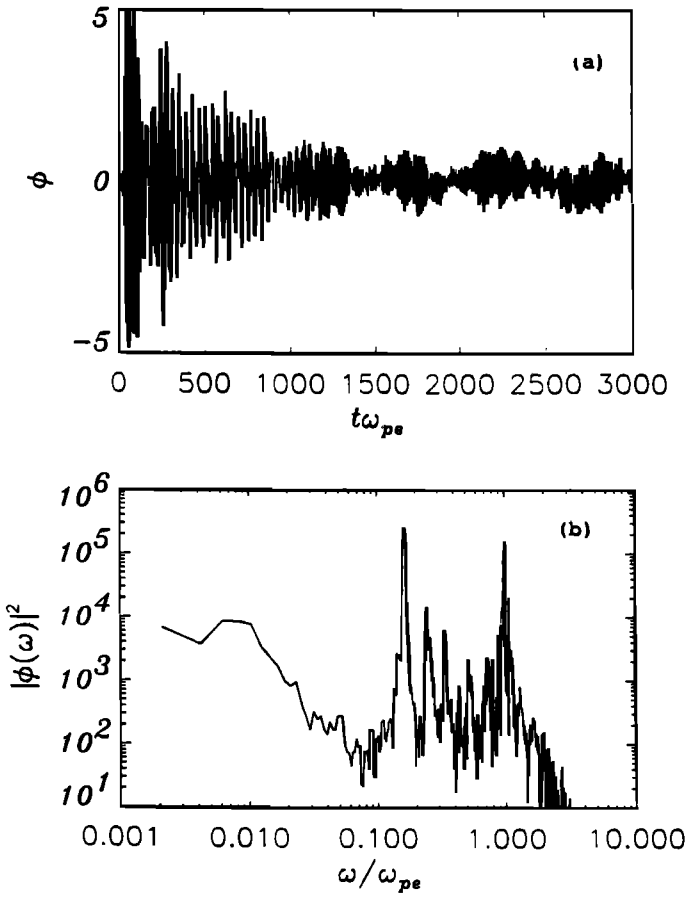


**Figure 1.** (a) Temporal evolution of the potential at point $P_1$ (16, 24, 5). Such a temporal evolution is typical of the entire plasma. (b) The Fast Fourier Transform of $\phi(t)$ in Figure 1a.

spectrum of the temporal variation of $\phi(t)$ at any point in the simulation volume. For example, the spectrum at another point $P_2$ is shown in Figure 2a; point $P_2$ (16, 16, 5) is transversely displaced from $P_1$. $P_2$ is near the center of the initial beam, while $P_1$ is near its edge. Note the spectra in Figures 1b and 2a are nearly identical except for some differences in the details. For the sake of ease in discussion, we separately describe the early ($\bar{t} < 900$) and late ($\bar{t} > 1000$) time evolutions of the waves in the following two subsections.

### 3.1. Early Time Behavior of the Waves

Figures 2b and 2c show the frequency spectrum for the oscillations at $P_2$ over a limited time interval $0 \le \bar{t} \le 900$. The spectra shown in these figures are the same except for the scale along the horizontal axis being logarithmic in Figure 2b and linear in Figure 2c. Comparing the spectra in Figures 2a and 2b, we see that they are nearly the same for $\omega_{lh} \le \omega \le \omega_{po}$, except for some essential difference in the fine structure near $\omega \sim \omega_{po}$, which will be discussed later. The most striking difference between the spectra in Figures 1b (or Figure 2a) and 2b is in the power levels at very low frequencies $\omega < \Omega_i$. The power at such frequencies is generated at times $\bar{t} > 900$; so it is significantly reduced in the spectrum for the earlier times ($\bar{t} < 900$) shown in Figure 2b. The generation of the low-frequency waves for $\omega \lesssim \Omega_i$ will be discussed in section 3.2.

The linear-frequency scale plot in Figure 2c reveals the details of the fine structure of the spectrum in Figure 2b; the largest power is near $\omega_o \cong \omega_{po}$, and then the next largest power is at a frequency $\omega_1 \cong 0.16\omega_{po} \cong 1.4\omega_{lh}$. The peak at this frequency is followed by the peaks at $\omega_2 = 0.25\omega_{po} = 2.2\omega_{lh}$, $\omega_3 = 0.34\omega_{po} = 3\omega_{lh}$, $\omega_4 = 0.43\omega_{po} = 3.9\omega_{lh}$, $\omega_5 = 0.52\omega_{po} = 4.7\omega_{lh}$, $\omega_6 = 0.75\omega_{po}$, $\omega_7 = 0.8\omega_{po}$, and $\omega_8 = 0.85\omega_{po}$. Then there are the peaks at $\omega > \omega_o$, and they are at $\omega_9 \approx 1.15\omega_{po}$, $\omega_{10} \sim 1.3\omega_{po}$, and $\omega_{11} \sim 1.7\omega_{po}$. Note that these latter peaks for $\omega > \omega_{po}$ are much broader. How are these various peaks generated, and what are the wave modes to which these peaks correspond? These are difficult questions to answer completely, but the major features of the spectrum in Figure 2c can be understood as explained below.

Figure 1a shows that at the very early times $\bar{t} \le 300$, the HF waves grow out to large amplitudes reaching $\bar{\phi}_m \sim 5$. The spatial structure of the HF waves at $\bar{t} = 100$ is shown in Figures 3a and 3b, in which the equipotential contours are plotted in the $x$-$z$ ($\bar{y} = 16$) and $y$-$z$ ($\bar{x} = 16$) planes, respectively. The dominant feature of the waves is that they are nearly periodic along the magnetic field $\mathbf{B}_o(\|z)$, and the dominant mode is determined by the wave vector components $k_\perp \sim 0$ and $k_\| = n2\pi/L_z$ with $n = 6$ for which parallel wavelengths are $\lambda_\| = 43\lambda_{do}$. Figure 3d shows the spatial

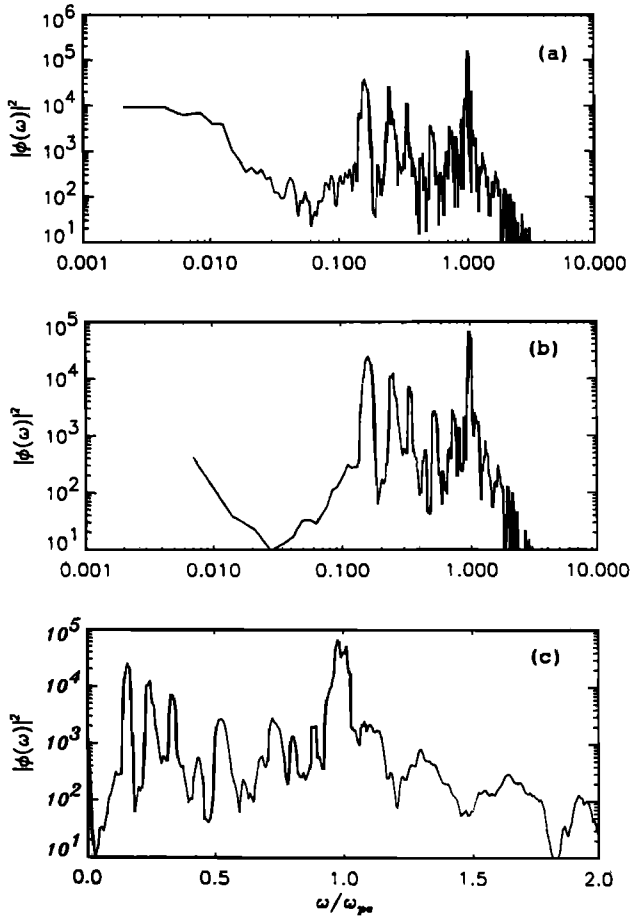


**Figure 2.** (a) Frequency spectrum of $\phi(t)$ at point $P_2$ (16, 16, 5) for the entire time interval $0 \le \bar{t} \le 3000$. (b) Same as Figure 2a but for $0 \le \bar{t} \le 900$. (c) Same as Figure 2b but for the horizontal scale being linear in frequency.

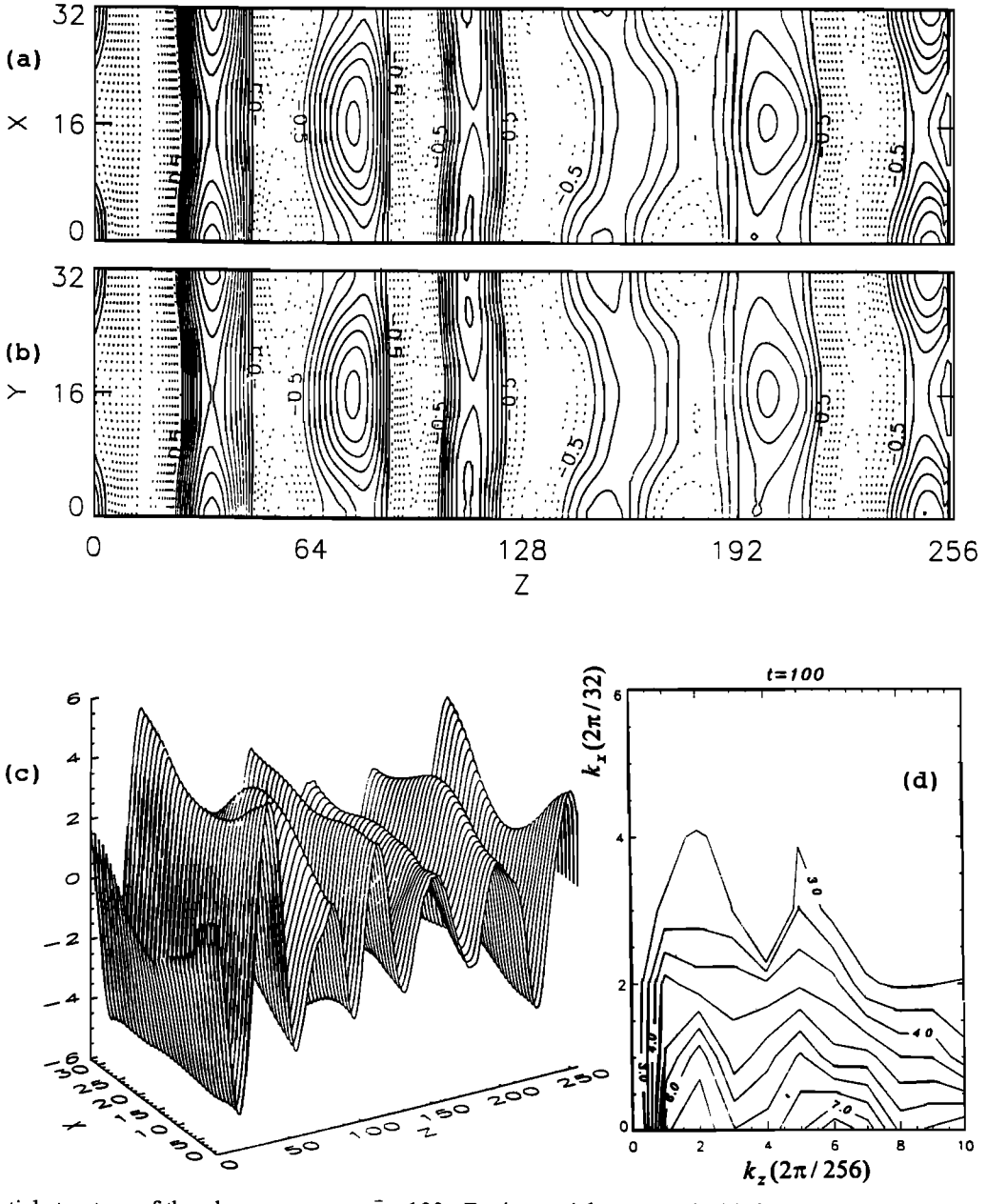


**Figure 3.** Spatial structure of the plasma waves at $\bar{t} = 100$. Equipotential contours in (a) the $x$-$z$ plane at $\bar{y} = 16$ and (b) the $y$-$z$ plane at $\bar{x} = 16$. In Figures 3a and 3b the solid contours show positive potentials while the dashed ones show negative potentials. The contour level –0.5 is the first dashed contour neighboring the positive ones. The contour levels are $\Delta\bar{\phi} = 0.5$ apart. (c) Surface plot of the potential distribution $\phi(x, y = 16, z)$ and (d) spatial Fourier components of the potential structure in Figure 3a. The components are described by the mode numbers $m$ and $n$ on the horizontal and vertical scales, giving $k_z$ and $k_x$, respectively. The contours show the power level on a relative log scale.

Fourier spectrum of the 2-D structure in Figure 3a, revealing the dominance of $k_\perp \cong 0$ and $k_\parallel = 6 \times 2\pi / L_z$. In Figure 3d there is an additional peak at $k_\perp = 0$ and $k_\parallel = 2 \times 2\pi / L_z$; this additional peak will be discussed later.

Since the beam density is $n_b \cong 0.1 n_o$, the target plasma density is $n_t = 0.9 n_o$ giving target plasma frequency $\omega_{pt} \cong 0.95 \omega_{po}$. The frequency of the Langmuir plasma oscillation with the above value of $k_\parallel$ and $k_\perp \cong 0$ is

$$\omega \cong \omega_{pt}(1 + 1.5 k_\parallel^2 \lambda_d^2) \cong 0.98 \omega_{po}. \quad (1)$$

This frequency is in good agreement with the peak just below $\omega/\omega_{po} = 1$ in Figure 2c. If this wave is resonantly driven by the beam electrons, it is resonant with electrons having parallel velocity $\bar{V}_\parallel \sim 7$, which is smaller than the initial beam velocity. Thus the HF waves at the early time are Langmuir waves supported by the ambient plasma and resonantly driven by the beam. The HF wave has some fine structure because of the modulations. Figure 1a clearly shows that prior to $\bar{t} \sim 300$ the wave has undergone amplitude modulations. Figure 3c shows the wave structure in Figure 3a as a surface plot of $\phi(x, 16, z)$ at $\bar{t} = 100$, revealing the corresponding spatial modulation. The perpendicular modulation gives rise to waves with nonzero perpendicular electric fields. Figures 3a-3c also reveal that the waves have

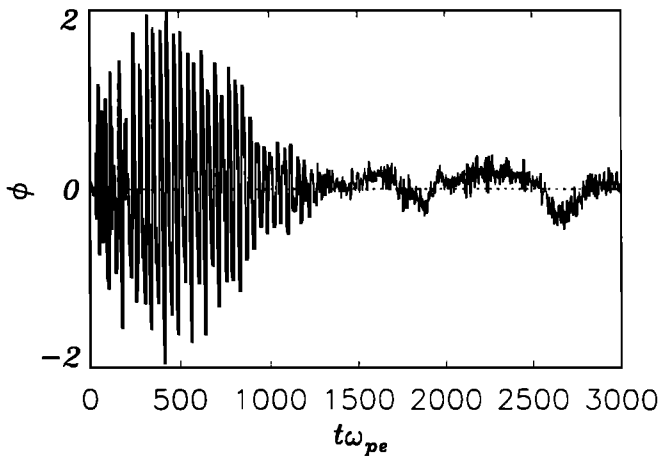


**Figure 4.** Temporal evolution of the potential at the point (16, 24, 5) when averaged over about an electron plasma period. Note that the oscillations for $\bar{t} < 1000$ are primarily at the frequency $\omega \cong \omega_l \cong 1.4\omega_{\ell h}$, and at later times the oscillations are slow and have frequencies $\omega < \Omega_i$.

undergone amplitude modulation in the parallel direction; the modulation has a wavelength of $\lambda_{\|} = 128\lambda_d$, corresponding to the peak at $k_{\|} = 2\times 2\pi/L_z$ in Figure 3d. The modulation of the HF waves prior to $\bar{t} = 300$ is representative of a strong interaction between the simultaneously excited HF and lower hybrid waves. The interaction leads to a near disappearance of the HF waves and a dominance of the LH waves over $300 < \bar{t} \sim 900$. We now demonstrate that the low-frequency waves modulating the HF waves and then dominating the wave spectrum are indeed the LH waves.

Figure 4 shows the same data as Figure 1a, except that it is averaged over $\Delta\bar{t} = 6$, which is about the electron plasma period; the averaging filters out the fast oscillations at frequencies near $\omega \cong \omega_{po}$, leaving the low frequencies unaffected. The averaged potential shows that for $\bar{t} \lesssim 1000$, the oscillations are primarily at $\omega \cong \omega_l \cong 0.16\omega_{po}$ as determined by the dominant wave period $\Delta\bar{t} \cong 40$. This is even more clearly demonstrated by the temporal behavior of the perpendicular electric field and its Fourier spectrum shown in Figures 5a and 5b for $E_x$. The LH wave dominates for $\bar{t} \lesssim 1000$ corresponding to the nearly monochromatic peak at $\omega \cong 0.16$ in Figure 5b. The significantly large power for $\bar{\omega} < \Omega_i \approx 0.03$ in the spectrum of Figure 5b corresponds to ELF waves, which we will discuss later. Note that the perpendicular fields are unaveraged data, unlike the averaged potential shown in Figure 4. This reveals that fast oscillations in $\phi$, dominating for $\bar{t} \lesssim 300$, are essentially parallel electric fields corresponding to the spatial variation of $\phi(z)$ (see Figure 3c), and at later times the transverse fields of the low-frequency LH and ELF waves dominate in the plasma. We

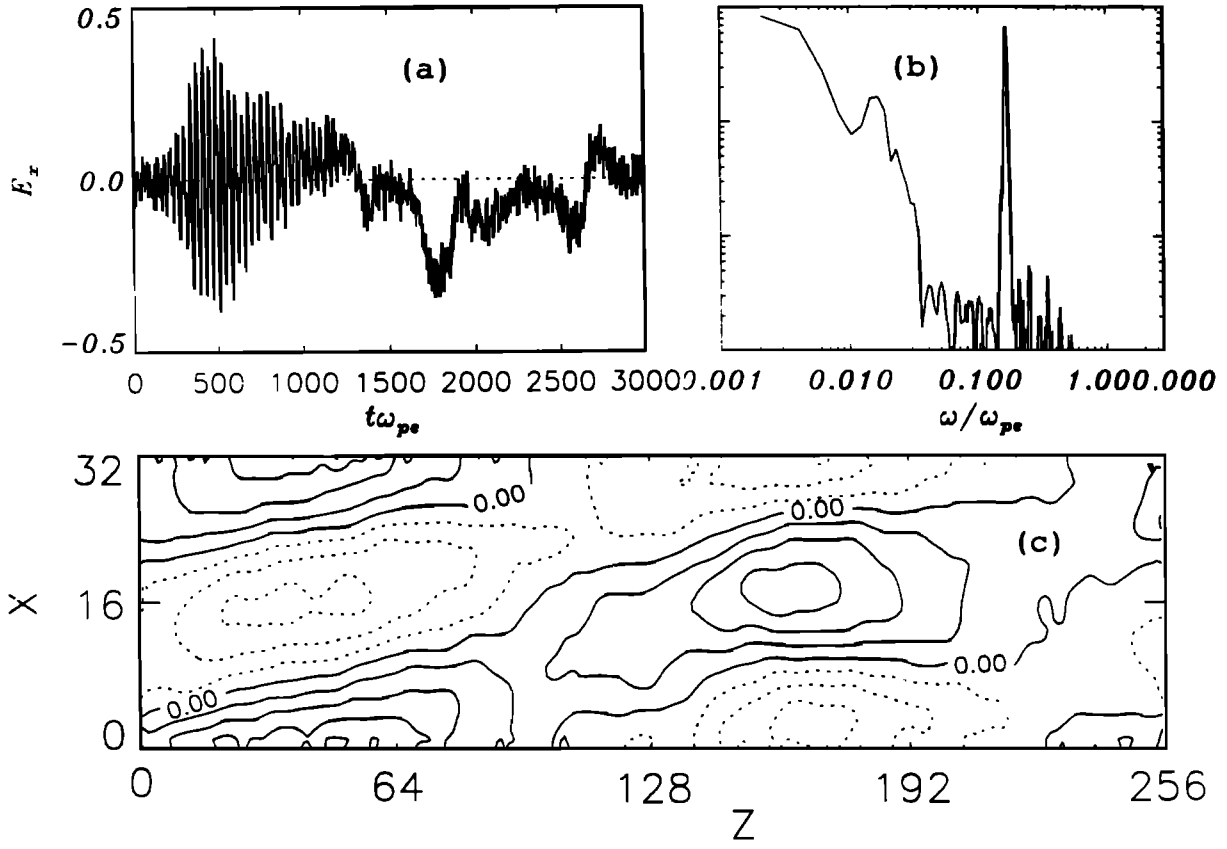


**Figure 5.** (a) Temporal evolution of the perpendicular electric field $E_x$ (16, 24, 5) and (b) its frequency spectrum showing a dominant peak at $\omega \cong \omega_l \cong 1.4\omega_{\ell h}$ and equally strong power levels at $\omega < \Omega_i \cong 0.03\omega_{po}$. Note that in Figure 5a the oscillations for $\bar{t} > 1000$ are the ELF waves corresponding to the frequencies $\omega < \Omega_i$. (c) Wave structure at $\bar{t} = 500$, when $E_x(t)$ nearly peaks in Figure 5a; contours of constant $E_x$ are plotted. The contour for $E_x = 0$ is labeled. The solid and dashed contours are for $E_x > 0$ and $E_x < 0$, respectively. The contour levels are $\Delta\bar{E}_x = 0.1$ apart.

now identify these low-frequency waves for $\bar{t} < 1000$. Figure 5c shows the wave structure in $E_x$ at $\bar{t} = 500$, when the amplitude of $E_x$ peaks in Figure 5a; contours of constant value of $E_x$ are plotted in this figure. The perpendicular wavelength of the wave is $\lambda_x \cong 32\lambda_{do}$, while $\lambda_{\|} \cong 256\lambda_{do}$, and the contours can be described by lines $x \cong (k_{\|}/k_x)z + c$, where $\bar{k}_{\|} = (2\pi/256)$ and $\bar{k}_{\perp} = (2\pi/32)$ and $c$ is a constant. The slopes of the lines fit nicely with the slopes of the contours in Figure 5c barring some localized perturbations. For the above values of $k_{\|}$ and $k_{\perp}$, the wave frequency for a LH mode is given by

$$\omega \cong \omega_{\ell h}[1 + (M/m)(k_{\|}/k_x)^2]^{1/2} \cong 1.4\omega_{\ell h}. \quad (2)$$

This is precisely the peak frequency $\omega \cong \omega_1$ in Figures 1b, 2a-2c, and 5b. A similar behavior of $E_y$ is also found. Thus the dominant wave over the time period $300 < \bar{t} < 1000$ is identified as the LH wave. How is this wave driven? The parallel phase velocity of the LH wave $\bar{V}_{\ell h} \cong \bar{\omega}/\bar{k}_{\|} \cong 6.5$. Thus, the waves are resonantly driven at a stage of the beam evolution when the initial beam is sufficiently spread out to have significant slope in the parallel velocity distribution function at $\bar{V}_{\|} \cong \bar{V}_{\ell h}$. It is worth pointing out here that if the LH waves were excited by the fan instability supported by a plateaued electron beam [e.g., *Omelchenko et al.*, 1994], the AECR velocity $\bar{V}_c = 82$. This is not possible in the simulation.

When the LH wave has grown sufficiently, its interaction between the LH and HF waves produces the two sidebands at $\omega \cong \omega_{hf} \pm \omega_{\ell h}$, corresponding to $\omega_8 \sim 0.85\omega_{po}$ and $\omega_9 \sim 1.15\omega_{po}$, the HF sidebands seen in the spectrum of Figure 2c mentioned earlier. The interaction involves scattering of HF waves on the LH wave oscillations, leading to the perpendicular modulations of the former. *Stasiewicz et al.* [1996] invoked a similar process involving the interaction of LH and HF waves for explaining observations of waves from Freja. The modulation leads to the changes in the wave structure for the HF waves; the wave vector matching condition requires that for the sidebands the parallel and perpendicular wave vector components satisfy the resonance conditions $k_{\|s} \cong k_{\|o} \pm k_{\|,\ell h}$ and $k_{\perp s} + k_{\perp \ell h} = 0$, where the subscripts $s$, $o$ and $\ell h$ correspond to the HF sidebands, the original HF wave, and the LH wave, respectively. Since $k_{\|,\ell h} \cong 2\pi/256 << k_{\|o}$, the sidebands should have nearly the same parallel wave number as the original HF waves. The perpendicular wave number of the scattered HF waves turns out to be just negative of the LH waves.

For the early time wave evolution discussed above, Figures 6a and 6b show the electron phase space in $z$-$V_z$ plane at $\bar{t} = 100$ and 400. The phase space plot at $\bar{t} = 100$ shows that there are well-formed vortexes corresponding to the wave structure in Figures 3a-3c. The vortexes are like electron-holes, but they do not last for a long time; they quickly dissipate, plateauing the electron beam as is apparent from Figure 6b for $\bar{t} = 400$. Figure 6c shows the velocity distribution in the $V_z$-$V_x$ plane. The important feature of the velocity distribution is the formation of the extended plateau in $V_z$, but the beam electrons also have undergone perpendicular heating as revealed by the transverse width of the plateau along $V_x$.

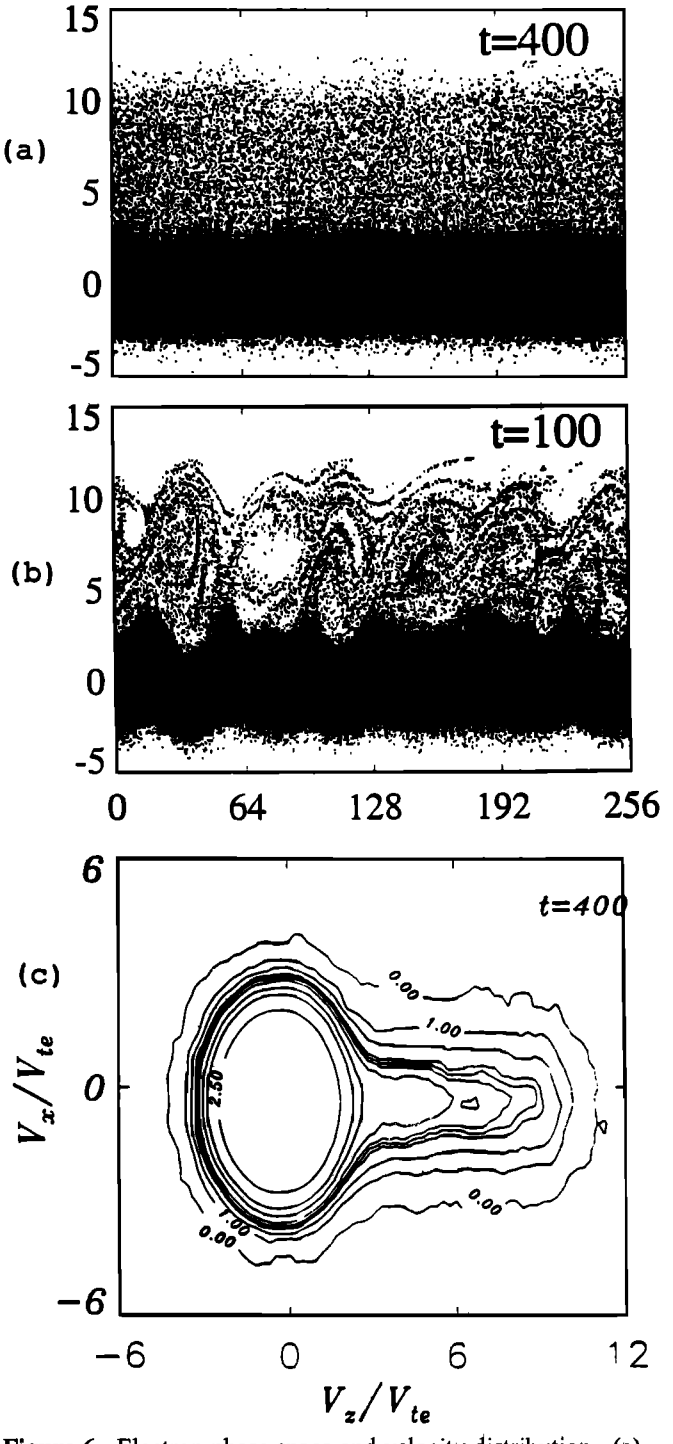


**Figure 6.** Electron phase space and velocity distribution. (a) $z - V_z$ phase space showing vortexes involving the beam electrons at $\bar{t} = 100$. (b) Same phase space at $\bar{t} = 400$, when the vortex structures have dissipated. (c) Velocity distribution $f(V_x, V_z)$ shown by contours of its constant values. The contour levels are on a relative log scale; all contours between those labeled with 2.5 and 1 are equispaced with an interval of 0.2.

### 3.2. Late Time Evolution

For the purpose of discussion here, the late time evolution refers to times $\bar{t} \geq 900$. As seen in Figure 1a, the evolution of the waves for such times is quite different from that for the earlier time $\bar{t} < 900$, when HF waves were a notable feature of the waves for $\bar{t} < 300$ followed by the dominance of a purely LH wave for $300 < \bar{t} < 900$. The data in Figure 1a are replotted for the time interval $900 \leq \bar{t} \leq 3000$ in Figure 7a on

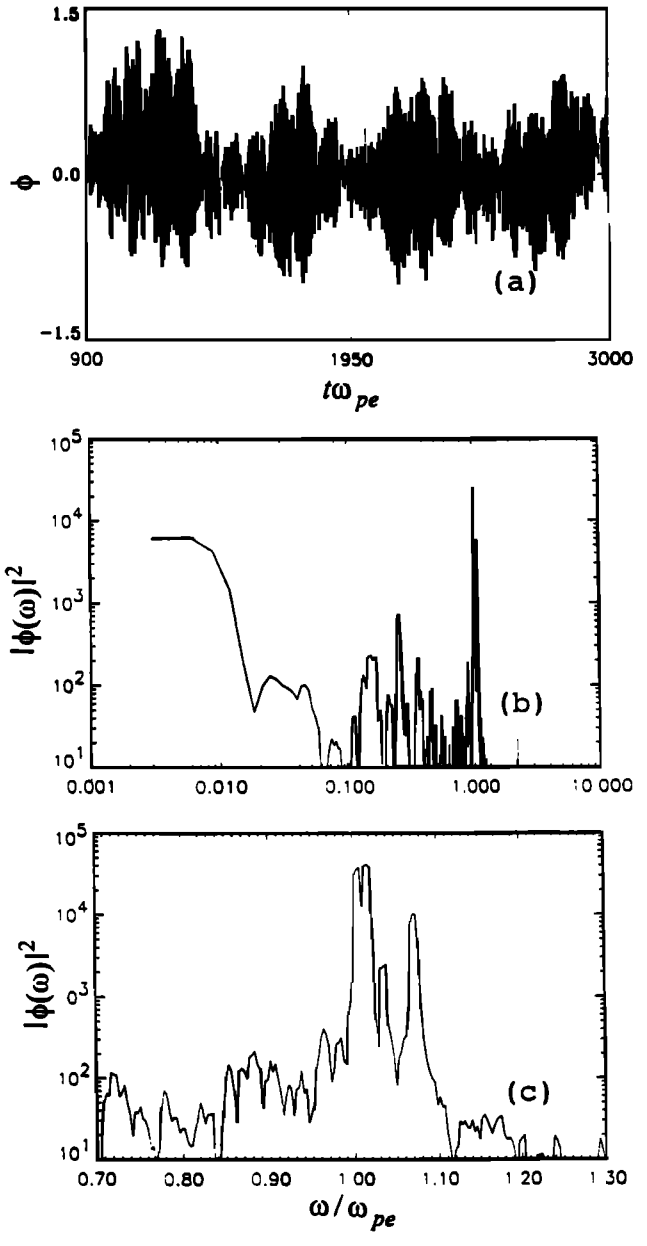


**Figure 7.** (a) Time evolution of the potential at point $P_1$ (16, 24, 5) for $900 < \bar{t} < 3000$. The data shown here are the same as in Figure 1a, but the vertical scale is expanded to clearly show the modulation of the HF waves at multiple timescales. (b) Frequency spectrum of the data plotted in Figure 7a. (c) Same as Figure 7b, but with a linear horizontal scale from $\omega = 0.7\omega_{pe}$ to $1.3\omega_{pe}$.

expanded vertical as well as horizontal scales, clearly showing that the HF wave has reemerged, and it is modulated by several low-frequency oscillations. Figure 7b shows the frequency spectrum of the data in Figure 7a. The HF waves are clustered around $\omega \sim \omega_{po}$. Furthermore, the spectrum contains a significant level of power at frequencies well below the ion cyclotron frequency $\Omega_i \cong 0.033\omega_{po}$.

The modulations over the time period $900 < \bar{t} < 1250$ (Figure 7a) have relatively small time periods corresponding to the LH waves at $\omega_L \cong 0.16\omega_{po}$ and $0.25\omega_{po}$; when such waves interact with the HF waves, sidebands at $\omega_s \cong \omega_{po} \mp \omega_L$ are generated. Figure 7c shows the spectrum of Figure 7b in the frequency range from $0.7\,\omega_{po}$ to $1.3\,\omega_{po}$ on a linear horizontal scale. Corresponding to the low frequencies $\omega_L$, the lower sidebands at $0.75\,\omega_{pe}$ and $0.84\,\omega_{pe}$ and an upper sideband at 1.16 are present in the spectrum of Figure 7c.

Figure 7c shows a dominant upper sideband at $\omega \cong 1.07\,\omega_{po}$ and a relatively weak lower sideband at $\omega \cong 0.93\,\omega_{po}$. These two sidebands of the dominant peak at $\omega \cong \omega_{po}$ correspond to the modulation at the time interval $\Delta\bar{t} \cong 90$, clearly seen in Figure 7a after $\bar{t} > 1200$.

In addition to the modulation with the timescale $\Delta\bar{t} \cong 90$, the HF waves are also modulated at another much longer timescale of about $\Delta\bar{t} \sim 550$ for which the modulating frequency is about $\omega_{elf} \cong (2\pi/550)\omega_{po} \cong 0.01\,\omega_{po}$. Figure 7b shows that for $\omega \leq 0.02\,\omega_{po}$, there is enhanced power level. The effect of the modulation at this long time scale is the split in the main HF peak, representing two sidebands at $\omega = \omega_{po} \pm \omega_{elf}$ with separation $\Delta\omega \cong 2\omega_{elf} \sim 0.02$.

The above discussion of Figures 7a-7c shows that in the late stage of the waves driven by an electron beam there are relatively low amplitude HF waves near $\omega \sim \omega_{po}$ with several sidebands, and correspondingly there are LF oscillations at frequencies in the range of ion cyclotron frequency ($\Omega_i$) and its harmonics and extremely low frequencies below $\Omega_i$.

In an attempt to understand the waves modulated in time, we begin with an examination of the evolution of the plasma

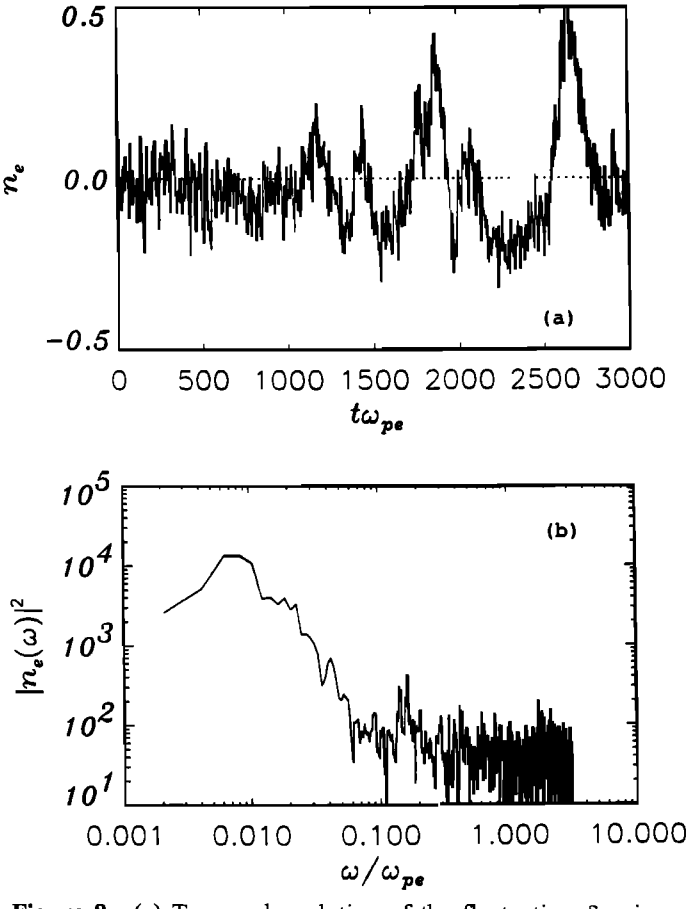


**Figure 8.** (a) Temporal evolution of the fluctuation $\delta n_e$ in the electron density at point $P_1$ (16, 24, 5), and (b) frequency spectrum of the data plotted in Figure 2a. Note the dominance of ELF oscillations with a time period $\Delta\bar{t} \sim 500$.

density. Figure 8a shows an example of the evolution of the electron density, and the corresponding Fourier spectrum is shown in Figure 8b. The electron density shown here is averaged over $\Delta\bar{t} \cong 6$, which tends to eliminate the fast HF oscillations. Only the LH and slower oscillations appear here. If we average out the LH oscillations, we see that slow ELF oscillations begin to grow as early as $\bar{t} \cong 500$, when the LH wave peaks as seen from Figures 4 and 5a. It appears that LH waves parametrically drive the ELF waves. The dispersion relation for the parametric process considered here is given by (see, e.g., *Shapiro* [1998])

$$\omega^2 = \omega_{pe}^2 \frac{k_\parallel^2}{k_\perp^2}\left[(\Omega_i^2/\omega_{pi}^2) - k_\perp^2\rho_i^2 \overline{W}_e \frac{\omega_{pe}^2/\Omega_e^2}{(1+\omega_{pe}^2/\Omega_e^2)} \frac{\mathbf{k}\times\mathbf{k}_o}{k^2 k_o^2}\right]$$

$$\times\left[\frac{k^2}{(\mathbf{k}_o-\mathbf{k})^2}\frac{1}{(\Delta_- + 2\omega/\omega_{\ell h})} + \frac{k^2}{(\mathbf{k}_o-\mathbf{k})^2}\frac{1}{(\Delta_+ - 2\omega/\omega_{\ell h})}\right] \quad (3)$$

where

$$\overline{W}_e = \tfrac{1}{2}\varepsilon_o E_{\perp o}^2 / n_o k_B T_o , \quad (4)$$

$\rho_i$ is the ion Larmor radius, $\mathbf{k}_o$ is the wave vector of the LH pump wave, $E_{\perp 0}$ is the amplitude of the perpendicular electric field of the pump (it stands for $E_x$ or $E_y$), $\mathbf{k}$ is the wave vector of the ELF wave with components $k_\parallel$ and $k_\perp$, $\omega$ is the frequency of the ELF wave, and $\Delta_\pm$ are the mismatches between the frequency of the LH pump and the frequencies of the LH satellites with the wave vectors $\mathbf{k}_o \pm \mathbf{k}$. We point out that the dispersion relation in (3) is the electrostatic version of the dispersion relation given by *Shapiro* [1998] describing the coupling of a LH pump wave with the inertial Alfven wave. *Roy and Lakhina* [1985] have performed similar analytical studies showing generation of ion cyclotron and very low frequency waves by the modulation instability of LH waves. In the electrostatic limit $k_\perp^2 c^2/\omega_{pe}^2 >> 1$, the inertial Alfven wave is described by (see, e.g., *Singh* [1999])

$$\omega \cong \omega_a \cong (k_\parallel/k_\perp)(M/m)^{1/2}\Omega_i . \quad (5)$$

This relation for $\omega_a$ is also identical to the frequency of the Bernstein mode for $n = 0$ [*Bhatia and Lakhina*, 1980]. In the limit $\overline{W}_e \to 0$, (3) reduces to (5).

Assuming $\Delta_\pm \sim \omega_a$, $k_\perp >> k_\parallel$ for both the LH and ELF waves, (3) can be written as

$$\omega^4 - (5/4)\omega_a^2\omega^2 + \omega_a^4/4 - \Gamma = 0 , \quad (6)$$

where

$$\Gamma = \tfrac{1}{2}\overline{W}_e \rho_i^2 k_\parallel^2 \frac{\omega_{pe}^4}{\omega_{pe}^2+\Omega_e^2}\omega_{LH}\,\omega_a . \quad (7)$$

The solution of (6) gives

$$\omega^2 = \tfrac{5}{8}\omega_a \pm \tfrac{1}{2}\sqrt{\tfrac{25}{16}\omega_a^4 + 4(\Gamma - \omega_a^4/4)} . \quad (8)$$

In the limit $\Gamma \to 0$, $\omega \cong \omega_a$ is one of the two solutions in (8). We note that when $\Gamma > \omega_a^4/4$, $\omega^2 < 0$ and the parametric process yields an aperiodic instability showing growth of the ELF waves. This occurs when $\overline{W}_e$ exceeds a threshold value given by

$$\overline{W}_{th} = (\omega_a/\Omega_i)\left(\frac{\Omega_i}{\omega_{pi}}\right)^3 \frac{(1+\Omega_e^2/\omega_{pe}^2)}{\rho_i^2 k_\perp^2} \quad (9)$$

In the simulation we find that $\omega_a/\Omega_i \sim 0.3$, $\omega_{pi}/\Omega_i = 4$, $\Omega_e/\omega_{pe} = 2$, and $\rho_i k_\perp \sim 1$ giving $\overline{W}_{th} \cong 0.02$. From Figure 5 we note that the maximum amplitude $E_{xo} \cong 0.4$, which yields $\overline{W}_e = 0.08$, well exceeding the above threshold.

In view of the above theoretical considerations we suggest that the LH waves efficiently couple to the ELF waves, and the coupling siphons the power from the former to the latter. This is clearly seen from Figure 5a. Figure 9a shows the temporal behavior of $E_y$ like that for $E_x$ in Figure 5a. The frequency spectrum of $E_y$ is shown in Figure 9b. For $\bar{t} < 900$, $E_y$ is dominated by LH waves and, at later times, by the ELF waves. The $E_x$ component (Figure 5a) acts as a pump for the $E_y$ component of the ELF waves in Figure 5b. Likewise the $E_y$ component of the LH wave (Figure 9a) acts as a pump for the $E_x$ component of the ELF wave in Figure 5a. This cross coupling is affected by the factor $(\mathbf{k}\times\mathbf{k}_o)$ in (3). Physically, this factor arises from the pondermotive force arising from the vector nonlinearity [*Shapiro et al.*, 1993].

We have so far considered the decay of the LH waves and the emergence of ELF waves. How do the HF waves reemerge? How is the modulation with timescale $\Delta\tilde{t} = 90$ generated?

We showed earlier the plateau formation in the electron velocity distribution function (Figure 6c). We find that the plateau, once formed, is not a static feature of the plasma; instead it evolves with time. Figures 10a–10c show the evolution of the plateau over one long LF modulation period in Figure 7a from $\bar{t} = 1000$ to 1400. The noteworthy feature of the evolution is the emergence of a beam-like feature with positive slopes imbedded in the plateau and its subsequent disappearance. The plateau has a very weak beam-like feature near $V_b \cong 8V_{te}$ when $\bar{t} = 1000$, but this feature grows to a well-formed beam at $\bar{t} = 1200$, and it disappears again at later times as shown in Figure 10c for $\bar{t} = 1400$. How does the beam-like feature re-form?

It is known that the plateau of the form in Figure 7c could generate waves via AECR [*Kadomstev and Pogutse*, 1968]. More recently, *Omelchenko et al.* [1994] renamed this mechanism for wave generation as the fan instability for generating LH waves. In view of very small $k_\parallel$ for LH waves, it takes very energetic electrons in the plateau to generate LH waves. But it is possible to excite other waves having relatively large values of $k_\parallel$. In our simulations, $\Omega_e = 2\omega_{pe}$, and for low frequencies $\omega < \omega_{\ell h}$, the AECR occurs for $k_\parallel > 2\omega_{pe}/V_\parallel \cong 0.25\lambda_d^{-1}$ for which parallel wavelengths are $\lambda_\parallel < 30\lambda_d$. Including the plateau, the effective electron temperature is $T_{\text{eff}} \cong 4T_o$, and the corresponding ion acoustic speed is $C_s = [(k_B T_{\text{eff}} + 3k_B T_o)/M]^{1/2} \cong 0.33V_{te}$. For the above parallel wave number the ion acoustic frequency $\omega \cong k_\parallel C_s \cong 0.07\omega_{pe}$, which falls just above $2\Omega_i$, the second ion cyclotron harmonic.

In the process of generating the low-frequency waves by AECR, electrons lose their parallel energy by $k_\parallel V_\parallel \hbar$, where $\hbar$ is Planck's constant, and most of this energy goes into the cyclotron motion because $\hbar\omega << \hbar k_\parallel V_b$. Thus electrons undergo an efficient pitch angle scattering. This leads to a slowing down of the resonant electrons in the parallel direction, and they bunch up just below the resonant parallel velocity, forming a beam-like feature. This process of retraction of the electrons in a plateaued beam was earlier studied by a number of authors, including *Shapiro and Shevchenko* [1968], *Parail and Pogutse* [1976], and *Muschietti et al.* [1981]. The emergence of the beam feature reexcites the fast HF oscillations. When these oscillations regrow, they replateau the reformed beam, and this process continues repeatedly.

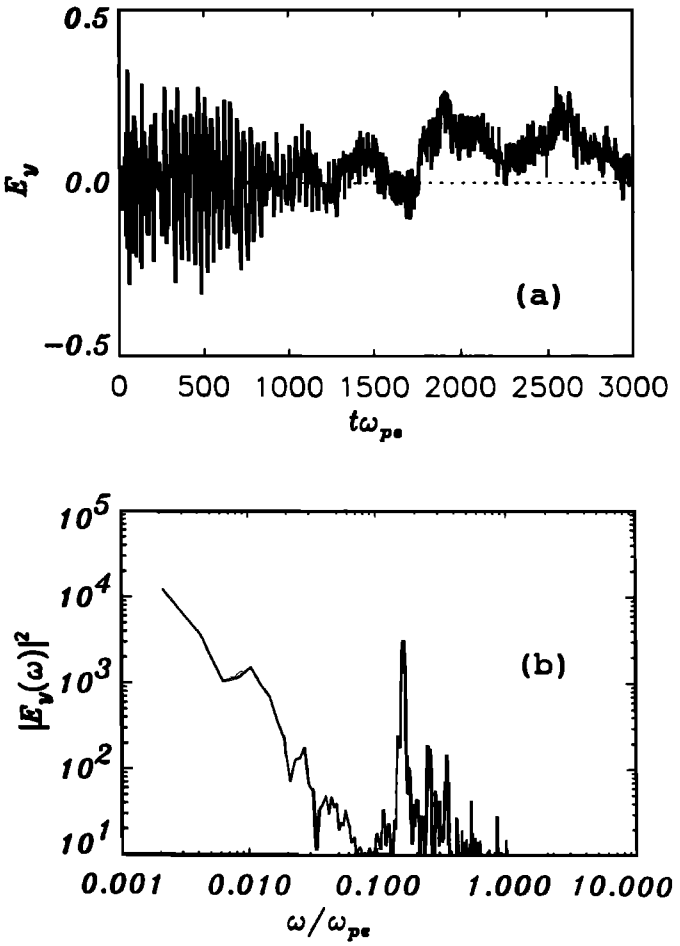


**Figure 9.** (a) Temporal evolution of $E_y$ at $P_1$ (16, 24, 5). (b) Frequency spectrum of data plotted in Figure 9a. As in Figure 5 for $E_x$, note that $E_y$ is dominated by LH waves for $\bar{t} < 900$ followed by the dominance of ELF waves.

The low-frequency waves generated by the AECR and the HF waves generated by the re-formed beam nonlinearly couple together to give the modulated waveform at the timescale of $\Delta\bar{t} \sim 90$, which is the time period of the ion acoustic wave with $\omega \cong k_{\|} C_s \cong 0.07\omega_{pe}$ discussed above. The result of this modulation is the prominent sideband at $\omega \cong 1.07\omega_{pe}$ and a weaker sideband at $\omega \cong 0.93\omega_{pe}$ in the spectrum of Figure 7c. The waveform resulting from this modulation is further modulated by the preexisting ELF waves, which resulted from the decay of LH waves.

### 3.3. Transformation of the Wave Structure From Early to Late Times

Figures 3a-3d showed the wave structure in the configuration space and in the wave vector space at an early time $\bar{t} = 100$. The dominant wave at this time is the one with $k_{\|} \cong 6 \times 2\pi/256$ and $k_{\perp} \cong 0$, although there is the beginning of modulation at smaller values of $k_{\|}$ and larger values of $k_{\perp}$. We have also shown that for $300 < \bar{t} < 900$, the LH waves dominate with predominantly perpendicular fields, and at even later times the ELF waves begin to dominate, and these later waves also have predominantly perpendicular fields. In order to contrast the wave structure at an early time against that at a later time, Figure 11a shows an example of potential structure in the $y$-$z$ plane at a late time. Figure 11b shows the associated structure in $E_y$, the perpendicular electric field component. These wave structures shown are at $\bar{t} = 2000$. In view of Figures 5a and 9a, the perpendicular field structure in Figure 11b belongs to the ELF oscillations. Note that the perpendicular field structure is characterized by short perpendicular and very long parallel scale lengths. The structures with relatively shorter parallel scale lengths in

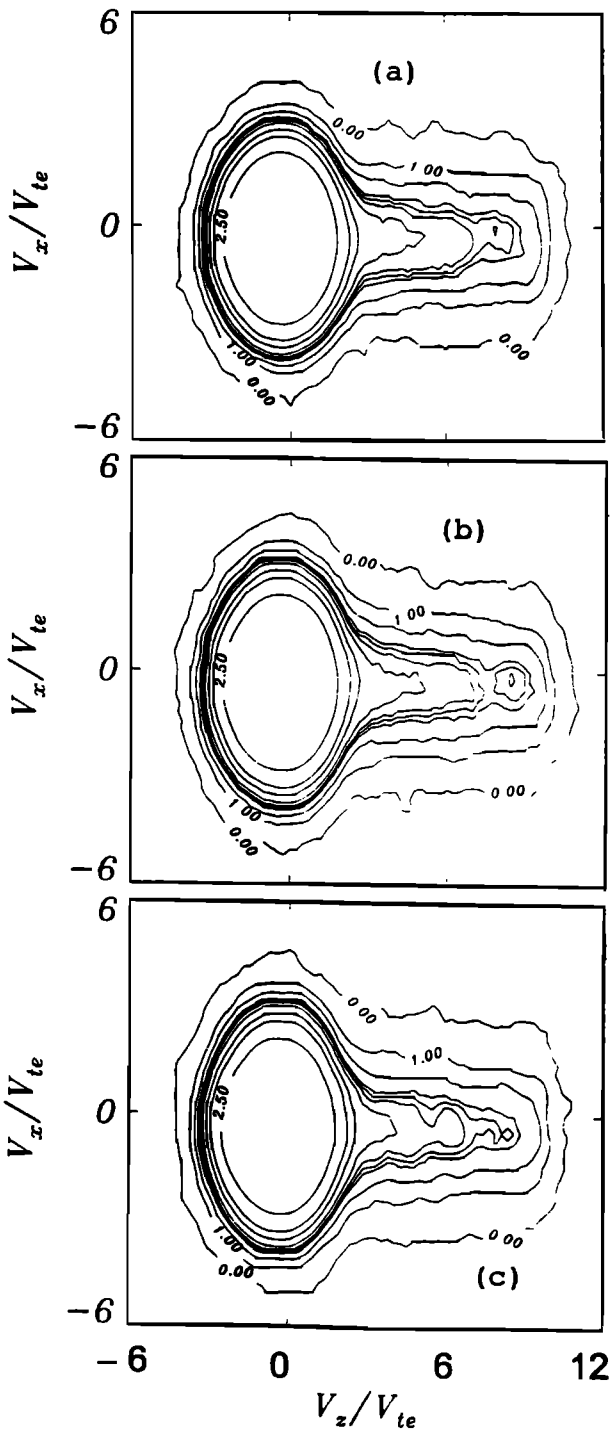


**Figure 10.** Temporal evolution of the plateaued electron beam: (a) $\bar{t} = 1000$, (b) $\bar{t} = 1200$, and (c) $\bar{t} = 1400$. Note the emergence of an electron beam near $\bar{V}_z \sim 8$ in Figure 10b. The contour levels are the same as in Figure 6c.

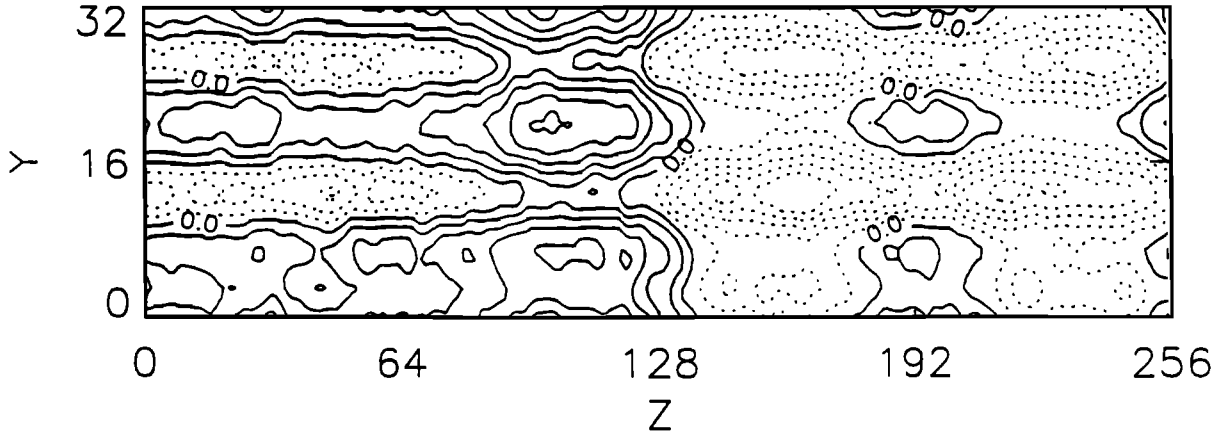


**Figure 11a.** Wave structure in $\phi(y, z)$ at $\bar{t} = 2000$. Note the contrast between the potential structure here and that at an early time shown in Figure 3b.

$\phi(y, z)$ (Figure 11a) belong to the HF oscillations of the parallel electric fields.

The above features of the transformation of the wave structure is nicely manifested in the transformation of the structure in the wave vector domain ($k$-domain). Figure 3d showed the wave structure in $k$-domain at $\bar{t} = 100$; further evolution in $k$-domain is shown in Figures 12a-12d. Note that in Figure 3d there is hardly any wave power for $\bar{k}_{\|} < 2\pi/256$, and most of the power is concentrated near $k_{\perp} \sim 0$ and $k_{\|} \cong 6 \times 2\pi/256$. In contrast, we note from Figures 12a-12d that the power is increasingly concentrated in the domain $\bar{k}_{\|} < 2\pi/256$, and it continually expands to larger values of $k_{\perp}$ until about $\bar{t} \cong 1200$, after which relatively large power extends up to $k_{\perp} \cong 8 \times 2\pi/32$ giving $\lambda_{\perp} \cong 4\lambda_d \sim \rho_i$, the ion Larmor radius. Figures 12a-12c show that there is a significant power at $k_{\|} \cong 6 \times 2\pi/256$ and $k_{\perp} \cong 0$ corresponding to the parallel HF wave with $E_{\|}$ oscillating at $\omega \sim \omega_{po}$, except at $\bar{t} \sim 2000$, when the HF wave has weakened considerably as seen from Figure 7a.

## 4. Consequences of the Plasma Waves

The plasma waves discussed in the above section have a great deal of influence on the energetics of both electrons and ions and on the structure of the plasma.

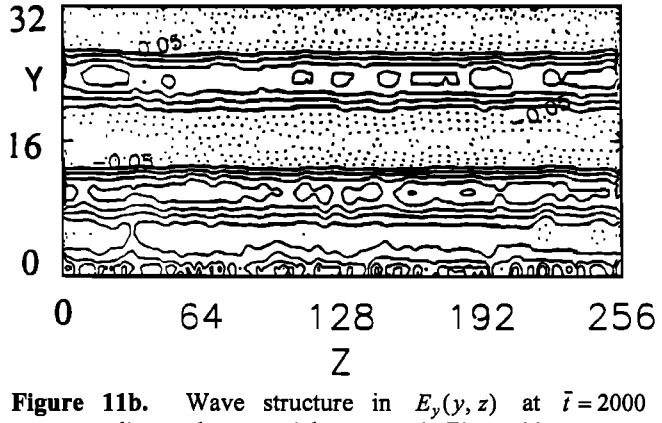


**Figure 11b.** Wave structure in $E_y(y, z)$ at $\bar{t} = 2000$ corresponding to the potential structure in Figure 11a.

### 4.1. Spatial distribution of Beam Electrons

Initially, at $\bar{t} = 0$, in the simulation described here, the cylindrical beam of radius $r_b = 10\lambda_{do}$ was centered ($(x-16)^2 + (y-16)^2 \leq 100$) in the simulation volume. We find that the beam electrons diffuse out of this initial volume and are progressively distributed throughout the entire volume of the simulation box. This is shown in Figure 13, in which the distributions of electrons in the $x - V_z$ phase space at $\bar{t} = 100$, 400, and 1000 are shown. Note that initially at $\bar{t} = 0$ there were only the thermal electrons for velocities $|\bar{V}_z| \leq 3$ and no beam electrons in the simulation volumes for $x \leq 6$ and $x \geq 26$. But by time $\bar{t} = 100$, the beam electrons have migrated outside the initial region and extend in $\bar{V}_z$ up to $|\bar{V}_z| \cong 12$. This trend continues as shown by the plot at $\bar{t} = 400$, and by time $\bar{t} = 1000$ the plateaued beam electrons occupy the entire simulation box with nearly the same spatial density as indicated by the nearly uniform density of the dots, representing electrons, for all values of $x$. In Figure 13 we show the distribution in $x$, but a similar distribution is found in any direction in the $x$-$y$ plane. Since the diffusion transverse to $\mathbf{B}_o$ is nearly completed by the time $\bar{t} \sim 1000$,, it is affected by the lower hybrid waves which dominate the plasma over this time interval. The primary cause of the cross-field diffusion is the shear in the $\mathbf{E} \times \mathbf{B}$ drift of electrons in the electric field fluctuations of the lower hybrid wave. The sheared drift associated with the spatial oscillations of $\mathbf{E}$ produces eddies in the electron flow. Such fluctuations randomize the transverse motion of the electrons causing the cross-field diffusion. *Chu et al.* [1975] have studied these nonlinear processes in detail showing anomalously enhanced cross-field diffusion of electrons and the damping of the lower hybrid fluctuations even in a plasma near thermal equilibrium. In a nonequilibrium plasma, like the situation studied in this paper, the anomalous effects are further enhanced.

### 4.2. Transverse Ion Heating

In the simulation discussed here, we find that the initial fast electron beam is able to transfer part of its parallel kinetic energy into transverse energy of few ions. Figure 14 shows the scatter plots of ions in $V_x - V_z$ plane at $\bar{t} = 400$ and 1000. The circularly symmetric distribution at $\bar{t} = 400$ is nearly the

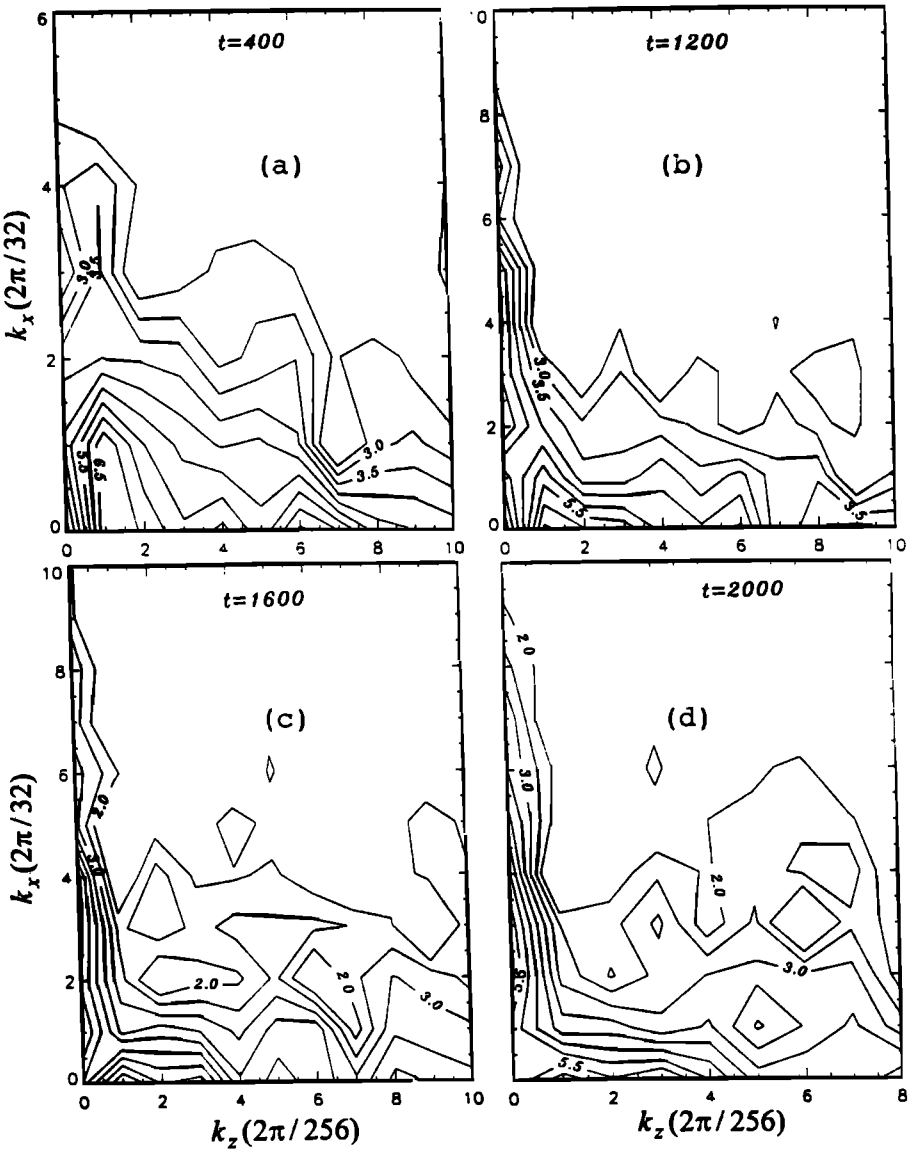


**Figure 12.** Wave structure in $k_z - k_x$ domain: (a) $\bar{t} = 400$, (b) $\bar{t} = 1200$, (c) $\bar{t} = 1600$, and (d) $\bar{t} = 2000$. Numbers on the horizontal and vertical scales are the mode numbers giving $\bar{k}_z = m(2\pi/256)$ and $\bar{k}_x = n(2\pi/32)$.

same as the initial distribution, showing no appreciable effect of the waves on the ions. The plot at $\bar{t} \sim 1000$ shows that some of the ions are affected by the waves resulting in transverse acceleration of the ions. We also note that the larger the transverse acceleration the larger is the parallel velocity of the ions. After $\bar{t} \sim 1000$, there is no significant change in the energetics of ions. Figure 15 shows the ion velocity distribution function $(F(V_x))$ at $\bar{t} = 0$ (solid line), 400 (dotted line), 1000 (dotted-dashed line), and 3000 (dashed line). The energization leads to the formation of an elongated tail in the transverse velocity. Note that appreciable energizations occur only after $\bar{t} = 400$, when LH waves are fully developed in the plasma (see Figures 4, 5, and 9). The acceleration nearly ends by the time $\bar{t} \sim 1000$, when the LH waves have considerably weakened in the plasma. The perpendicular phase velocity of the LH wave

$$V_{p\perp} \cong \omega/k_\perp \cong 0.15/0.2 = 0.75 V_{te} \cong 6 V_{ti} \qquad (10)$$

which falls just out of the tail of the initial ion population where there are hardly any ions (see Figure 14a). How are the ions accelerated? The acceleration occurs when the ions are trapped inside the growing potential of the LH waves. This acceleration process is known as the stochastic acceleration as discussed by *Karney* [1978] for ion acceleration by large-amplitude LH waves and further applied to the transverse ion heating of heavy $O^+$ and $He^+$ ions in the auroral plasma by the hydrogen cyclotron waves [*Singh et al.*, 1981, 1982, 1985; *Roy and Lakhina*, 1985; *Papadopoulos et al.*, 1980]. It is worth pointing out that even though the acceleration is affected by coherent waves, but the motion of the ions becomes a random process when the wave amplitude is sufficiently large. For this reason the acceleration has been termed stochastic in the literature. The acceleration occurs when the ions, perpendicular velocity exceeds a minimum velocity given by

$$V_{\perp o} = (\omega/k_\perp)(1 - \alpha^{1/2}/\nu), \qquad (11)$$

where $\nu$ is an integer closest to the ratio $\omega/\Omega_i$, the

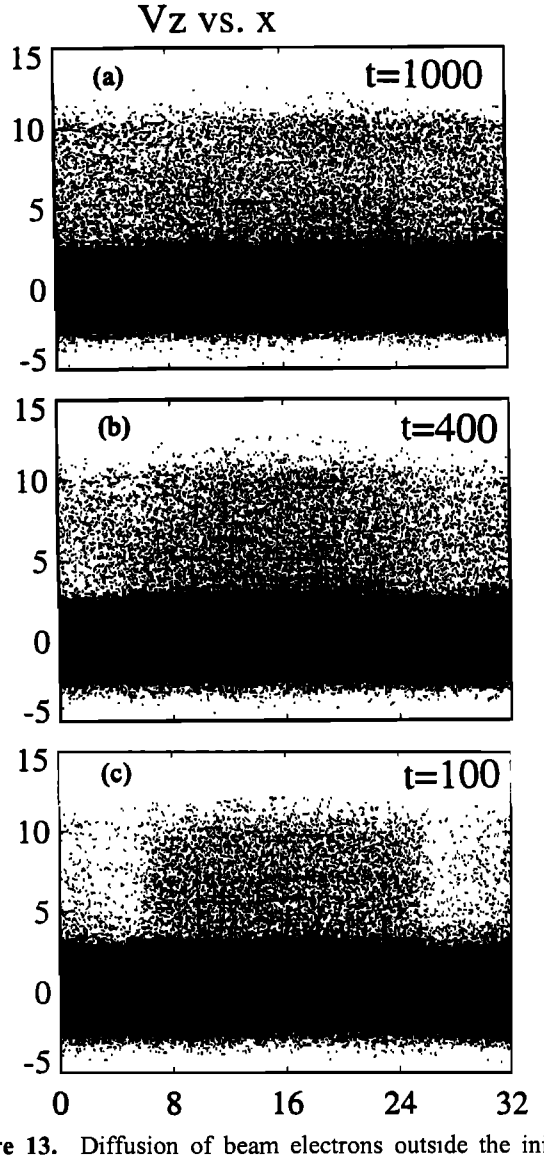


**Figure 13.** Diffusion of beam electrons outside the initial volume occupied by the beam. The diffusion is shown in the $x-V_z$ plane of the phase space at (a) $\bar{t}=1000$, (b) $\bar{t}=400$, and (c) $\bar{t}=100$. Note that as $t$ increases, the beam electrons progressively spread out of the initial volume $6<\bar{x}<26$, and at $\bar{t}\sim 1000$ the beam density becomes nearly constant as a function of $x$.

perpendicular phase velocity of the LH waves is $V_{p\perp}=\omega/k_\perp$, $\omega$ is the frequency of the LH waves, and

$$\alpha = k_\perp^2 e\phi_o / M\Omega_i^2 . \qquad (12)$$

The maximum acceleration occurs up to [e.g., see *Singh et al.*, 1981]

$$V_{\perp\max} \cong \frac{\Omega_i}{k_\perp}(4\nu\alpha)^{2/3}(2\pi)^{1/3} \qquad (13)$$

when the LH wave peaks in the simulation $\phi_o \cong 3.5\,(k_B T_e/e)$, and as was already discussed $\bar{k}_\perp = (2\pi/32)\lambda_d^{-1}$ and $\nu\sim\omega/\Omega_i\sim 5$. For these parameters we find that $V_{\perp o}\sim 0.5V_{te}\cong 4V_{ti}$, enabling the ions in the tail to undergo acceleration by the LH wave. The maximum acceleration is possible up to $V_{\perp\max}\cong 1.5V_{te}$. Figure 14b shows that the maximum acceleration is limited to $V_{\perp\max}\cong 1.2V_{te} < V_{\perp\max}$.

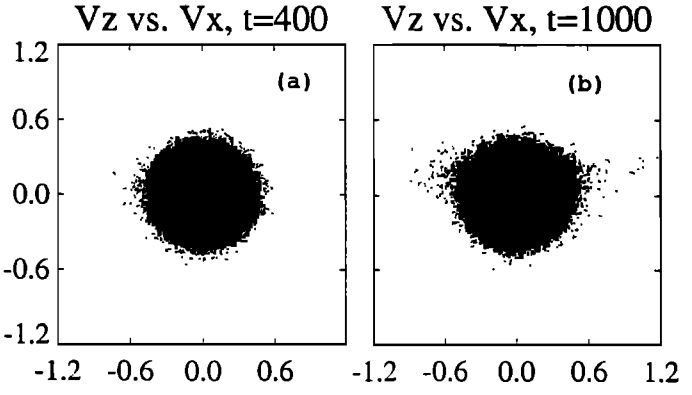


**Figure 14.** Scatter plots of ions in $V_x-V_z$ phase space: (a) $\bar{t}=400$ and (b) $\bar{t}=1000$. Note that the transverse acceleration of a few ions extending in $V_x$ up to $\sim 1.2V_{te}\cong 9.6V_{ti}$.

This is expected in view of the evolving wave amplitudes in the simulations.

It is important to point out that at later times when LH waves have considerably weakened and very low frequency waves for $\omega<\Omega_i$ dominate along with HF waves at $\omega\sim\omega_{po}$, there is hardly any further acceleration of ions, as shown by the comparison of curves for $\bar{t}=1000$ and 3000 in Figure 15.

### 4.3. Density Perturbation

In response to the wave dynamics discussed in section 3, the plasma density distribution is filamented; the filaments are narrow structures across $\mathbf{B}_o$ and quite elongated parallel to $\mathbf{B}_o$. As expected, the filaments consist of both density enhancements and depletions. Figure 16a shows the density structure at $\bar{t}=1000$ in the $y$-$z$ plane, when the LH waves have considerably weakened. The corresponding density structure in the $x$-$y$ plane at $\bar{z}=128$ is shown in Figure 16b. The lighter the shade in the grey scale plot the larger is the density, while for the darker shade the density is progressively lower. Note that the density filaments run all along the length of the plasma along $\mathbf{B}_o$; accordingly, the structure shown in Figure 16b is true for all $x$-$y$ planes in the simulation volume. In the $x$-$y$ plane, the depletions and the enhancements in the

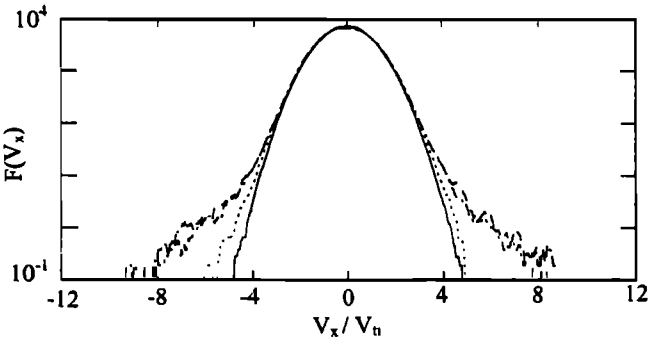


**Figure 15.** Velocity distribution functions of ions at several times; solid curve is for $\bar{t}=0$, showing the initial distribution function $F(V_x)$. The dotted, dotted-dashed, and dashed curves are for $\bar{t}=400$, 1000, and 3000, respectively. Note that the two latter curves nearly overlap, showing that the transverse acceleration saturates by the time $\bar{t}\sim 1000$.

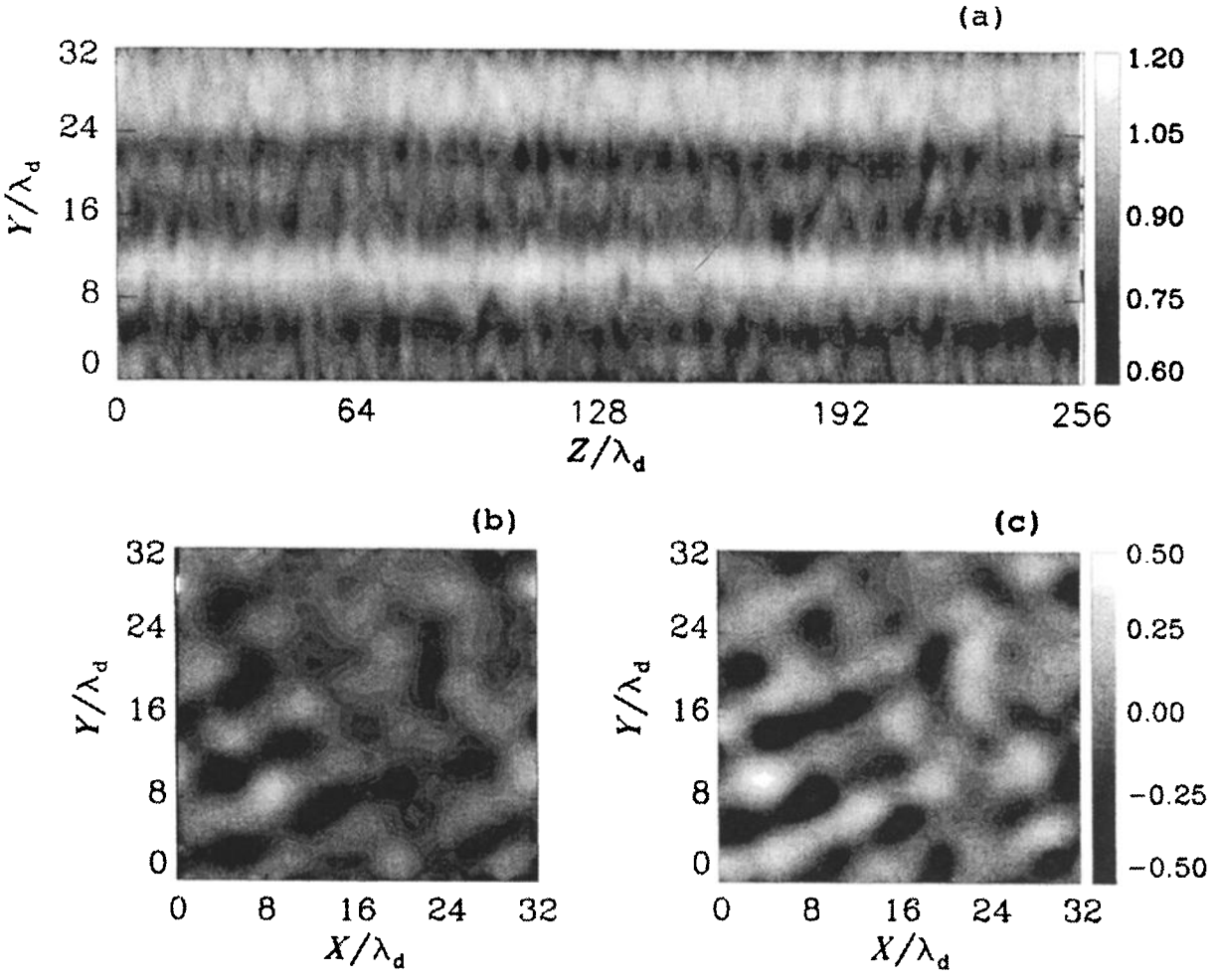


**Figure 16.** Density distribution in the simulation volume at $\bar{t}=1000$: (a) $y$-$z$ plane at $\bar{x}=16$, (b) $x$-$y$ plane at $\bar{z}=128$, and (c) spatial distribution of $\nabla\cdot\mathbf{E}_\perp$ in the same $x$-$y$ plane as in Figure 16b. Note the filamentation of the plasma density; the filaments are thin across $\mathbf{B}_o$ and extend all along the length of the simulation box parallel to $\mathbf{B}_o$.

density (Figure 16b) constitute a wave pattern with some quite localized enhancements and depletions in the density. The wave pattern is intimately related to $\nabla\cdot\mathbf{E}_\perp$, where $\mathbf{E}_\perp$ is the perpendicular electric field vector. The relationship between patterns in $\delta n_e(x,y)$ and $\nabla\cdot\mathbf{E}_\perp(x,y)$ can be seen by comparing Figure 16b with Figure 16c, in which $\nabla\cdot\mathbf{E}_\perp$ is shown in a grey scale plot. The darker (lighter) the region, the more negative (positive) $\nabla\cdot\mathbf{E}_\perp$ is. The early filamentation of the plasma density is a consequence of the coupling of the LH waves with the ELF waves discussed earlier. However, for $\bar{t}>900$, when the LH waves have considerably weakened and ELF waves dominate with oscillating perpendicular electric fields (Figures 5a and 9a), the density structures are associated with these oscillating fields. In view of the fact that the electrons are highly magnetized, a question arises as to how the electrons are transported across $\mathbf{B}_o$. The cross-field transport of electrons occurs via the electron drift velocity $V_D$ determined by the vector sum of the polarization and $\mathbf{E}\times\mathbf{B}$ drifts, namely,

$$V_D=(\frac{E_y}{B_o}\hat{a}_x-\frac{E_x}{B_o}\hat{a}_y)-\frac{1}{\Omega_e}\frac{1}{B_o}\partial\mathbf{E}_\perp/\partial t, \qquad (14)$$

where $E_x$ and $E_y$ are the components of the perpendicular electric field vector $\mathbf{E}_\perp$. Ions also undergo similar drifts. If we linearize the electron continuity equation, we find

$$\frac{\partial n_e}{\partial t}=-n_o\nabla\cdot\mathbf{V}_D=+(1/\Omega_e)(1/B_o)\frac{\partial}{\partial t}(\nabla\cdot\mathbf{E}_\perp) \qquad (15)$$

Note that divergence of the term in the parentheses in (14) is identically zero because this term is $(\partial E_y/\partial x-\partial E_x/\partial y)$, which is the $z$ component of $\nabla\times\mathbf{E}$, and it must vanish for the electrostatic fields. Thus the density variation of electrons is caused by the polarization drift. Equation (15) can be further written as

$$\delta n_e\cong(\omega_{pe}^2/\Omega_e^2)(\frac{\varepsilon_o}{e})\nabla\cdot\mathbf{E}_\perp. \qquad (16)$$

Likewise we can write for the perturbation in the ion density

$$\delta n_i\cong-(\omega_{pi}^2/\Omega_i^2)(\frac{\varepsilon_o}{e})\nabla\cdot\mathbf{E}_\perp. \qquad (17)$$

In the regions where $\nabla\cdot\mathbf{E}_\perp<0$, as in the dark regions in Figure 16c, $\delta n_e$ tends to become negative and $\delta n_i$ tends to be positive, both contributing to increasing the positive space charge there. This reverses the sign of $\nabla\cdot\mathbf{E}_\perp$ to be positive. Thus the density structure oscillates as shown in Figure 8a. Since the system is highly nonlinear, the above linear analysis is not expected to explain all the features in the density oscillations.

### 4.4. Relevance of Density Perturbations to Lower Hybrid Solitary Structures

In a series of observations from rocket and satellite experiments lower hybrid solitary structures (LHSS) have been measured [e.g., *Kintner et al.*, 1992; *Schuck et al.*, 1998; *Pecseli et al.*, 1996; *Høymork et al.*, 2000]. The LHSS are transversely localized LH waves, which generally occur in a density depletion. The magnitude of the depletion ranges from a few percent to a few tens of percent. The measurement from Freja has shown that the transverse scale length is typically $\ell_\perp \sim 30$ m with a sharp lower cutoff at $\ell_\perp \sim 15$ m, and on the high side $\ell_\perp$ could be as high as ~70 [e.g., see *Høymork et al.*, 2000]. How do such density cavities form? This question has been debated since the beginning of their first observations [*Kintner et al.*, 1992]. Suggestions for explaining the LHSS phenomenon include LH wave collapse [*Shapiro et al.*, 1993; *Vago et al.*, 1992], parametric decay of LH waves [*Singh et al.*, 1998], cavitation by the mirror force [*Singh*, 1994], and thermal instability [*Pecseli et al.*, 1996]. *Schuck et al.* [1998] have demonstrated that scattering of the background LH waves by a preexisting density depletion produces the main feature of the LHSS as measured in the rocket experiments.

Our simulation results presented here show that the formation of plasma striations with density enhancements and depletions are a common feature of a plasma permeated by an electron beam. They result from the parametric decay of lower hybrid waves into the ELF waves. In a previous paper we reported generation of density striations when a LH pump wave decayed into ion cyclotron waves, in contrast to the LH waves being directly driven by an electron beam [*Singh et al.*, 1998]. These studies show that LH waves create their own density perturbations in the course of their nonlinear evolution.

In the initial value simulations discussed here, the LH waves decay away in the course of the formation of the ELF density striations, and the waves do not persist as enhanced structures inside the perturbations. However, if there was a renewed source for the excitation of the LH wave, for example, in the form of a fresh electron beam in the simulation after the formation of the ELF striations, it is quite possible that newly generated waves can get trapped in the existing density structures as shown by *Schuck et al.* [1998].

It is worthwhile to examine the scale lengths and the propagation characteristics of the ELF wave density perturbations and compare them with similar features of the LHSS recently reported by *Høymork et al.* [2000], who have presented a statistical study of the Freja data on the transverse scale length of a cavity and have shown that the LHSS move transversely with a velocity of ~1km/s.

As was mentioned earlier, the ELF waves considered here are the electrostatic approximation of the inertial Alfven (IA) waves. Including the warm plasma effects the, IA waves are described by the dispersion relation (see, e.g., *Lysak* [1998])

$$\omega^2 = k_\parallel^2 V_A^2 \frac{1+k_\perp^2\rho_a^2}{1+k_\perp^2/k_s^2}, \tag{18}$$

where $V_A$ is the Alfven velocity; $\rho_a$ is an effective scalelength defined by $\rho_a = \rho_i(3/4 + T_e/T_i)$ with $\rho_i$ as the ion Larmor radius, $T_e$ and $T_i$ are the electron and ion temperatures, respectively; and $k_s = \omega_{pe}/c$, where $c$ is the velocity of light. For $T_e >> T_i$, $\rho_a$ becomes the ion Larmor radius with the ion acoustic speed given by $C_a = (k_B T_e/M)^{1/2}$. In the electrostatic approximation $k_\perp^2 >> k_s^2$, (18) becomes

$$\omega \cong k_\parallel V_A (k_\perp^{-2} + \rho_a^2)^{1/2}/\lambda_s, \tag{19}$$

where $\lambda_s$ is the collisionless skin depth given by $\lambda_s = 1/k_s = c/\omega_{pe}$. When $k_\perp^2\rho_a^2 << 1$, (19) gives the cold plasma electrostatic resonance cone waves for $\omega << \Omega_i$ as given by (5). In view of the observational results of *Høymork et al.* [2000], it appears that $\lambda_s^2 >> k_\perp^{-2} >> \rho_a^2$, for which the cold plasma electrostatic ELF wave approximation is indeed valid. Under this approximation, the perpendicular group velocity of the waves

$$V_{g\perp} = \left|\partial\omega/\partial k_\perp\right| = (k_\parallel/k_\perp)(M/m)^{1/2}\Omega_i/k_\perp. \tag{20}$$

Assuming that waves are below the $O^+$ ion cyclotron frequency $\Omega_{O^+}$, we can estimate the group velocity of the waves as follows. Assuming that $\omega << \Omega_{O^+}$, say, $\omega/\Omega_{O^+} = 0.1$, we find that $k_\perp/k_\parallel = (M/m)^{1/2}(\Omega_{O^+}/\omega) = 1714$. For the typical scale length of $\ell_\perp \sim k_\perp^{-1} \cong 30$ m, we find that corresponding parallel scale length $\ell_\parallel \cong 52$ km. For $\Omega_{O^+} = 180$ rad/s, $V_{g\perp} \cong 540$ m/s. *Høymork et al.* [2000] report that the LHSS move transversely to the ambient magnetic field with such small velocities.

The parallel phase velocity of the ELF wave is given by

$$V_{p\parallel} = \omega/k_\parallel = (M/m)^{1/2}\Omega_i/k_\perp.$$

For the parameters used in calculating $V_{g\perp}$, we find that for $\ell_\perp \sim k_\perp^{-1} = 30$ m, $V_{p\parallel} \cong 928$ km/s, which should be compared with the electron thermal velocity $V_{te}$. Høymork et al. report that electron temperature $T_e \cong 3000°$ K for which $V_{te} \cong (k_B T_e/m)^{1/2} \cong 340$ km/s. Thus for $L_\perp \sim 30$, $V_{p\parallel} \cong 3V_{te}$. When $\ell_\perp \lesssim 15$ m, $V_{p\parallel} \lesssim 1.5V_{te}$, for which there should be a strong Landau damping by the electrons, possibly explaining why there should be a sharp lower cutoff near $\ell_\perp \cong 15$ m.

Summarizing the above discussion, we note that properties of the electrostatic resonance cone wave density perturbations match well with the measured properties of the density cavities associated with the LHSS; these properties include their perpendicular scale length and perpendicular motion. Furthermore, we have shown that for $\ell_\perp \lesssim 15$ m, the ELF waves will be heavily Landau-damped, establishing the lower bound on the scale length of the density perturbation associated with LHSS. The upper bound on $\ell_\perp$ is perhaps the collisionless skin depth. However, when $\ell_\perp \to \lambda_s$, the ELF waves become electromagnetic in nature and then the amplitude of the density perturbation is fairly weak, and it may not be strong enough to affect the trapping and scattering of LH waves. In contrast, the electrostatic waves for $\ell_\perp << \lambda_s$ carry with them sufficiently strong density depletions to strongly interact with a background LH wave as shown by *Schuck et al.* [1998].

It is important to comment on the fact that the electrostatic ELF waves have both density enhancement and depletions as in a wave motion. In contrast, the LHSS are generally seen in density depletions. Previously, we have pointed out that the symmetry between the density depletions and enhancements can be broken by the mirror force, which acts on the plasma particles when they are transversely accelerated [*Singh*, 1994; *Singh et al.*, 1998]. The mirror force causes density evacuation; which deepens the density depletions and reduces the amplitude of the density enhancements.

## 5. Conclusion and Discussion

The main purpose of this paper is to study the nonlinear behavior of the plasma and waves driven by an electron beam of finite radius across the ambient magnetic field. We found that the beam initially drives both high-frequency waves near $\omega \sim \omega_{po}$ and low-frequency waves near the lower hybrid frequency $\omega \sim \omega_{lh}$. The two waves nonlinearly couple, the latter modulating the former. The changing plasma conditions lead to the weakening of the HF waves and dominance of the LH waves. When the LH waves begin to dominate, the HF waves appear as an additive noise to the LH waveform. Such behavior of HF and LH waves was reported by *Stasiewicz et al.* [1996] on the basis of observations from Freja in the auroral plasma at an altitude of $\cong 1400$ km. The observed waves were driven by electrons accelerated in narrow structures of kinetic Alfven waves. *Stasiewicz et al.* have discussed that the nonlinear interaction producing the waveform of the HF waves modulated by the LH waves could be a result of either a scattering of the HF waves by preexisting LH waves or a parametric decay of the former into the latter. The simulations show that for thin electron beams the LH waves and HF waves grow simultaneously, producing the modulated waveforms. Furthermore, our simulations show that the LH waves prevail over much longer times when driven by an electron beam compared with the lifetime of the large-amplitude HF waves. This is in agreement with the observational feature that the LH waves are more commonly observed wave modes than the HF mode. This has led *Stasiewicz et al.* to hypothesize that the modulated HF waves are probably the result of scattering of HF waves by preexisting LH waves.

We have also shown here that the LH waves, when fully developed, transversely heat the ions. The heating occurs by the chaotic motion of the ions in large-amplitude LH waves. Thus the nonlinearity brings about the Stochastic behavior of ions resulting into heating as proposed by *Karney* [1978] and applied to ion heating in space plasmas by *Papadopoulos et al.* [1980], *Singh et al.* [1981, 1982, 1985], and *Roy and Lakhina* [1985]. The heating is limited to the ions in the tail of the ion velocity distribution function. This is the first time we have shown here that an electron beam drives LH waves, accelerating ions transversely without any restriction on the angles of propagation of the waves as previously done by *Reterrer and Chang* [1988].

The simulation results suggest that the LH waves parametrically decay into ELF waves which occur for $\omega < \Omega_i$. Even though our simulation is electrostatic, it is relevant to the generation of ELF waves commonly observed in the auroral plasma. If such waves are directly driven by an electron beam with positive slopes [see *Cattell et al.*, 1998; *Temerin and Lysak*, 1984; *Singh et al.*, 1985], the question remains as to why the positive slopes are not already destroyed by much faster growing waves at higher frequencies such as the LH and HF waves. Our simulation shows that an electron beam of finite radius simultaneously drives LH and HF waves. When the LH waves are grown to sufficiently large amplitude, they decay into ELF waves by a modulational instability. We have given an analytical treatment for the decay process. Our treatment is similar to the calculations of *Shapiro* [1998] in which he has shown how LH waves lead to the generation of inertial Alfven waves. In the electrostatic limit the inertial Alfven waves become the ELF wave seen in the simulations. In this respect, our simulation verifies the analytical calculations of *Shapiro* [1998]. It is important to note that once the ELF waves emerge from the LH waves, they persist for a long time. Another important consequence of the LH waves is the diffusion of electrons from inside the initial beam volume to the outside regions [*Chu et al.*, 1975].

Once the electron beam has been plateaued, the HF wave again begins to appear in the simulation. Such HF waves in the late stage of the simulation ($\bar{t} > 1000$) are modulated by a variety of waves with different timescales, ranging from very large time periods of the ELF waves to the relatively short time periods of the LH, ion acoustic, and probably the ion cyclotron harmonic waves. We find that the plateau in the parallel electron velocity distribution is highly dynamic; periodically, it develops a small positive slope. We have explained this as being due to the electron dynamics affected by the AECR [*Kadomstev and Pogutse*, 1968]. In the process of driving the low-frequency waves, the AECR causes pitch angle scattering of the electrons in the plateau. The pitch angle scattering bunches the electrons at relatively small parallel velocity, creating a positive slope in the parallel velocity distribution. This generates the HF waves. These waves nonlinearly interact with the other low-frequency waves, generating the modulated waveform at late times. At such late times, the perpendicular electric field primarily has quite low-frequency components $\omega \lesssim \Omega_i$, while $E_{\|}$ has frequency components near $\omega \sim \omega_{po}$.

It is worth pointing out that our simulation shows a dramatic transformation of the wave structures as time progresses after initialization of the electron beam in the plasma. At very early times ($\bar{t} < 100$), waves are primarily parallel polarized; that is, the wave fronts are nearly transverse to the ambient magnetic field ($\mathbf{B}_o$), or the normal to the wave fronts ($\mathbf{k}$) is nearly parallel to $\mathbf{B}_o$. As time increases and various nonlinear wave interactions ensue, the normal ($\mathbf{k}$) to the wave fronts become increasingly oblique to $\mathbf{B}_o$, and at late stages the normal becomes nearly perpendicular to $\mathbf{B}_o$. It is important to note that a similar feature of wave transformation was studied by *Muschietti et al.* [1997] purely on the basis of quasi-linear treatment of wave generation by an electron beam in the presence of a hot electron halo in the electron velocity distribution function. In our simulation the transformation from nearly parallel (HF) waves to nearly transverse waves occurs without the hot electron halo.

In addition to the transverse ion heating, an important consequence for the plasma due to the nonlinear evolution of the waves is that the plasma density undergoes oscillations at the ELF frequency. The spatial structure of the plasma density associated with these oscillations is like filaments, which extend all along the length of the simulation plasma parallel to $\mathbf{B}_o$, but they are quite thin transverse to $\mathbf{B}_o$. We have shown that the major features of Freja data on LHSS [see *Høymork et al.*, 2000] are explainable in terms of the electrostatic ELF wave structure, including the upper and lower bounds on the perpendicular scale length and their perpendicular motion.

Finally, we point out that here we have performed electrostatic simulations. Therefore the electromagnetic effects are missing. Our comparison of ELF waves with waves in the frequency band $\omega < \Omega_i$ is only approximate;

such waves have a significant electromagnetic component when the perpendicular wavelengths are comparable to or larger than the collisionless skin depth $\lambda_e$. Furthermore, we mention that so far our simulations have been run as an initial value problem in which the electron beam is initialized at time $\bar{t} = 0$. In some applications, the plasma needs to be continuously driven by a fresh electron beam. In future simulations we hope to overcome these limitations. Only after fully electromagnetic and driven simulations have been performed might it be possible to interrelate a diverse set of phenomena such as the generation of LH waves, their nonlinear evolution into "ELF" and Alfven waves, and the scattering of the LH waves by the self-consistently generated density structures.

**Acknowledgements.** This work was preformed under NASA grant NAG54604 and NSF grant ATM9814571. The simulations were performed at JPL's Exemplar machine. The authors gratefully acknowledge help from Edith Huang in the process of running the code on the JPL machines. N. Singh acknowledges the hospitality at the Indian Institute of Geomagnetism, Colaba, Mumbai, where part of this work was prepared. We dedicate this paper to the fond memory of our longtime colleague and friend Heinz Thiemann.

Janet G. Luhmann thanks Vitali Shapiro and another referee for their assistance in evaluating this paper.

## References

Bhatia, K. G., and G. S. Lakhina, Low-frequency electrostatic instability due to anti-loss-cone electrons, *J. Plasma Phys., 24*, 221, 1980.

Cattell, C., et al., The association of electrostatic ion cyclotron waves, ion and electron beams and field-aligned currents: FAST observations of an auroral zone crossing near midnight, *Geophys. Res. Lett., 25*, 2053, 1998.

Chang, R. P. H., and M. Porkolab, Parametrically induced nonlinear wave-particle scattering and plasma heating near the lower hybrid frequency, *Phys. Rev. Lett., 32*, 1227, 1974.

Chang, T., Lower hybrid collapse, caviton turbulence and charged particle energization in the topside ionosphere and magnetosphere, *Bull. Am. Phys. Soc., 37*, 1407, 1992.

Chang, T., and B. Coppi, Lower hybrid acceleration and evolution in the suprauroral region, *Geophys. Res. Lett., 8*, 1253, 1981.

Chu, C., J. M. Dawson, and H. Okuda, Anomalous electron transport and lower-hybrid wave damping, *Phys. Fluids, 18*, 1762, 1975.

Ergun, R. E., G. T. Delory, E. Klementis, C.W. Arlson, J. P. McFadden, I. Roth, and M. Temerin, VLF wave growth from dispersive bursts of field-aligned electron fluxes, *J. Geophys. Res., 98*, 3777, 1993.

Høymork, S. H., H. L. Pecseli, B. Lybekk, J. Trulsen, and A. Eriksson, Cavitation of lower hybrid waves in the Earth's ionosphere: A model analysis, *J. Geophys. Res., 105*, 18,519, 2000.

Kadomstev, B. B., and O. P. Pogutse, Electric conductivity of a plasma in a strong magnetic field, *Sov. Phys. JETP, Engl. Tansl. 26*(6), 1146, 1968.

Karney, C. F. F., Stochastic ion heating by a lower hybrid wave, *Phys. Fluids, 21*, 1584, 1978.

Kintner, P. M., J. Vago, S. Chesney, R. L. Arnoldy, K. A. Lynch, C. J. Pollock, and T. E. Moore, Localized lower hybrid acceleration of ionospheric plasma, *Phys. Rev. Lett., 68* (16), 2448, 1992.

Klumpar, D. M., Transversely accelerated ions: An ionospheric source of hot magnetospheric ions, *J. Geophys. Res., 84*, 4229, 1979.

Lysak, R. L., Comment on "Theory of nearly perpendicular electrostatic plasma waves and comparison to Freja satellite observations," by C. E. Seyler and J.-E. Wahlund, *J. Geophys. Res., 103*, 7043, 1998.

McFadden, J. P., et al., Electron modulation and ion cyclotron waves observed by FAST, *Geophys. Res. Lett., 25*, 2045, 1998.

Mikhailovskii, A. B., *Theory of Plasma Instabilities, Vol. 1*, pp. 172-173, Plenum Publishing Company, New York, 1974.

Muschietti, L., K. Appert, and J. Vaclavik, Cerenkov and anomalous Doppler effects in the relaxation of an electron beam, *Phys. Fluids, 24*(1), 151, 1981.

Muschietti, L., I. Roth, and G. Delory, Oblique turbulence driven by field-aligned electron fluxes in the auroral ionosphere, *J. Geophys. Res., 102*, 27,217, 1997.

Omelchenko, Y. A., V. D. Shapiro, V. I. Shevchenko, M. Ashour-Abdalla, and D. Schriver, Modified lower hybrid fan instability excited by precipitating auroral electrons, *J. Geophys. Res., 99*, 5965, 1994.

Omura, Y., H. Matsumoto, T. Miyake, and H. Kojima, Electron beam instabilities as generation mechanism of electrostatic solitary waves in the magnetotail, *J. Geophys. Res., 101*, 2685, 1996.

Papadopoulos, K., J. D. Gaffey Jr., and P. J. Palmadesso, Stochastic acceleration of large (*M/q*) ions by hydrogen cyclotron waves in the magnetosphere, *Geophys. Res. Lett., 7*, 1014, 1980.

Parail, V. V., and O. P. Pogutse, Instability of the runaway-electron beam in a tokamak, *Sov. J. Plasma Phys., 2*, 125, March-April 1976.

Pecseli, H. L., K. Iranpour, O. Holter, B. Lybekk, J. Holtet, J. Trulsen, A. Eriksson, and B. Holback, Lower-hybrid wave cavities detected by the Freja satellite, *J. Geophys. Res., 101*, 5299, 1996.

Reterrer, J. M., and T. Chang, Plasma simulation of intense VLF turbulence and particle acceleration in the suprauroral region, in *Physics of Space Plasmas*, edited by T. Chang, p. 309, Scientific, Gainesville, FL, 1988.

Rosenberg, S., and W. Gekelman, Electric field measurements of directly converted lower hybrid waves at a density striation, *Geophys. Res. Lett., 25*, 865, 1998.

Roy, M., and G. S. Lakhina, Lower hybrid wave model for aurora, *Astrophys. Space Sci., 117*, 111, 1985.

Schuck, P. W., C. E. Seyler, J.-L. Pincon, J. W. Bonnell, and P. M. Kintner, Theory, simulation, and observation of discrete eigenmodes associated with lower hybrid solitary structures, *J. Geophys. Res., 103*, 6935, 1998.

Serizawa, Y., and C. T. Dum, Nonlocal analysis of finite-beam-driven instabilities, *Phys. Fluids B 4*, 2389, 1992.

Shapiro, V. D., Modulational interaction of the lower-hybrid waves with a kinetic-Alfven mode, *Phys. Rev. Lett., 81*(16), 3415, 1998.

Shapiro, V. D., and V. I Shevchenko, Quasilinear theory of relaxation of an electron beam in a magnetoactive plasma, *Sov. Phys. JETP, Engl. Transl., 27*(4), 635, 1968.

Shapiro, V. D., et al., Wave collapse at the lower hybrid resonance, *Phys. Fluids B, 5*, 31148, 1993.

Singh, N., Pondermotive versus mirror force in creation of thin filamentary cavities in auroral plasma, *Geophys. Res. Lett., 21*, 257, 1994.

Singh, N., Field patterns of Alfven wave resonance cones, *J. Geophys. Res., 104*, 6999, 1999.

Singh, N., and R.W. Schunk, Energization of ions in auroral plasma by broadband waves: Generation of conics, *J. Geophys. Res., 89*, 5538, 1984.

Singh, N., R. W. Schunk and J. Sojka, Energization of ionosphere ions by electrostatic hydrogen cyclotron waves, *Geophys. Res. Lett., 8*, 1249, 1981.

Singh, N., R. W. Schunk and J. Sojka, Cyclotron resonance effects on stochastic acceleration of the light ionospheric ions, *Geophys. Res. Lett., 9*, 1053, 1982.

Singh, N., R. W. Schunk and J. J. Sojka, Preferential perpendicular acceleration of heavy ionospheric ions by interaction with electrostatic hydrogen cyclotron waves, *J. Geophys. Res., 88*, 4055, 1983.

Singh, N., J. R. Conrad, and R. W. Schunk, Electrostatic ion cyclotron, beam-plasma, and lower hybrid waves excited by an electron beam, *J. Geophys., Res., 90*, 5159, 1985.

Singh, N., B. E. Wells, A. Abdelrazek, S. Al-Sharaeh, and W. C. Leung, Three-dimensional kinetic simulation of the nonlinear evolution of lower hybrid pump waves, *J. Geophys. Res., 103*, 9333, 1998.

Singh, N., S. M. Loo, B. E. Wells, and C. Deverapalli, Three-dimensional structure of electron holes driven by an electron beam, *Geophys. Res. Lett., 27*, 2469, 2000.

Stasiewicz, K., et al., Parametric instabilities of Langmuir waves observed by Freja, *J. Geophys. Res., 101*, 21,515, 1996.

Temerin, M. J., and R. L. Lysak, Electromagnetic ion cyclotron mode (elf) waves generated by auroral electron precipitation, *J. Geophys. Res.*, *89*, 2849, 1984.

Vago, J. L., P. M. Kintner, S. W. Chesney, R. L. Arnoldy, K. A. Lynch, T. E. Moore, and C. J. Pollock, Transverse ion acceleration by localized lower hybrid waves in the topside auroral ionosphere, *J. Geophys. Res.*, *97*, 16,935, 1992.

G. S. Lakhina, Indian Institute of Geomagnetism, Colaba, Mumbai, India. (lakhina@iig.iigm.res.in)

S. M. Loo, N. Singh, and B. E. Wells, Department of Electrical and Computer Engineering, College of Engineering, University of Alabama in Huntsville, Huntsville, AL 35899. (smloo@ece.uah.edu; singh@ece.uah.edu; wells@ece.uah.edu)

(Received August 31, 2000; revised November 29, 2000; Accepted January 12, 2001.)